An arms race under RIG-I loss: 5'ppp-RNA and its alternative recognition receptor MDA5

Shang Geng[1], Xing Lv[1], Weiwei Zheng[1], Tianjun Xu[1,2,*]

1. *Laboratory of Fish Molecular Immunology, College of Fisheries and Life Science, Shanghai Ocean University, Shanghai, China*
2. *Laboratory of Marine Biology and Biotechnology, Qingdao National Laboratory for Marine Science and Technology, Qingdao, China*

*Corresponding author. Dr. Tianjun Xu

E-mail: tianjunxu@163.com

Running title: MDA5 and 5'ppp-RNA

Abstract: The incessant arms race between viruses and hosts has led to numerous evolutionary innovations that shape the evolution of life. During this process, the interactions between viral receptors and viruses have garnered significant interest since viral receptors are cell surface proteins exploited by viruses to initiate infection. To further understand the interaction between viruses and receptors, our study sheds light on the arms race between the MDA5 receptor and 5'ppp-RNA in vertebrates. Firstly, the frequent and independent loss events of RIG-I in vertebrates prompted us to search for alternative immune substitutes, with homology-dependent genetic compensation response (HDGCR) being the main pathway. Our further analysis suggested that MDA5, the homolog of RIG-I, can replace RIG-I in recognizing 5'ppp-RNA and bind STING for signal transduction, which may lead to redundancy of RIG-I and loss from the species genome during evolution. Secondly, as an adversarial strategy, 5'ppp-RNA SCRV can utilize the m^6A methylation mechanism to degrade MDA5 and weaken its antiviral immune ability, thus promoting its own replication and immune evasion. In summary, our study has revealed the molecular mechanisms underlying the interaction and coevolution between vertebrate and virus, which providing valuable insights into the ecological and evolutionary factors that contribute to the diversity of the immune system.

Keywords: RIG-I; MDA5; 5'ppp-RNA; Genetic compensation response; Pattern recognition receptors; Immune evasion

1. Introduction

Pattern recognition receptors (PRRs) can be classified into three main groups: toll-like receptors (TLRs), retinoic acid-induced RIG-I-like receptors (RLRs), and NOD-like receptors (NLRs). The PRRs recognize conserved pathogen-associated molecular pattern (PAMP) motifs, including proteins, lipids and nucleotides, resulting in activation of innate immune responses of host[1]. TLRs are located on the cell membrane and recognize PAMPs outside the cell, while RLRs and NLRs are located within the cytoplasm and recognize PAMPs inside the cell. RLRs are a specific group of PRRs belonging to the family of DExD/H-box RNA helicases, and they play a crucial role in the innate antiviral response. There are three members in the RLR family: retinoic acid-inducible gene I (RIG-I), melanoma differentiation-associated gene 5 (MDA5), and laboratory of genetics and physiology 2 (LGP2). RIG-I and MDA5 exhibit similar signaling characteristics and structural homology, including two N-terminal caspase-recruitment domains (CARDs), a DExD/H box RNA helicase domain, and a C-terminal repressor domain (RD)[2]. However, LGP2 lacks CARD domain[2]. The specific roles of RIG-I and MDA5 in response to virus stimulation are not redundant: RIG-I detects short blunt-end RNA with a 5'-triphosphate motif (5’ppp-RNA), while MDA5 specifically recognizes long forms of viral dsRNA[3-5]. In contrast, the involvement of LGP2 in cytosolic RNA sensing remains a topic of debate. Some studies have proposed that LGP2 is crucial for the production of type □ interferon (IFN-□) in response to several RIG-I- and MDA5-dependent viruses[6], whereas others have described LGP2 as a negative regulator of RIG-I signaling[7]. However, surprisingly, despite the important immune functions of RLR members, they have been lost from the genome in many species including mammals, birds, and fish[8-10].

5’ppp-RNA contains a wide variety of RNA viruses, including Flaviviridae, Paramyxoviridae, Coronaviridae, Orthomyxoviridae, and Rhabdoviridae families[4]. These viruses widely infect all kinds of life and cause various harmfulness and serious diseases, and the infected hosts range from the highest vertebrates to the lowest vertebrate, teleost fish. In mammals, the harmfulness and serious diseases caused by many 5’ppp-RNA viruses in mammals are well known. For example, the genus *Lyssavirus* which belongs to the rhabdovirus infect only mammals and can cause fatal encephalitis (rabies)[11]. Moreover, the coronavirus is a highly infectious virus that can cause respiratory infections and potentially lead to severe health conditions, including pneumonia, acute respiratory distress syndrome, multiple organ failure, etc[12]. While in non-mammalian vertebrates, the interactions with the host by the 5’ppp-RNA viruses are not well known. 5’ppp-RNA viruses are expected to be recognized and trigger an antiviral immune response by RIG-I. However, RIG-I is lacking in many non-mammalian vertebrates, so who then recognizes 5’ppp-RNA in these species? One candidate gene that may play this role is yet unknown. When a gene is functionally inactive or lost, other genes or pathways may undergo genetic compensation response (GCR) to maintain organismal balance. One important mechanism to achieve GCR is through homology-dependent genetic compensation response (HDGCR), organisms often have the ability to intelligently evolve and utilize homologous genes to compensate for the functional loss caused by the loss of a certain gene. The pressure from viral infections has led to the evolution of the immune system, and the loss of RIG-I may be accompanied by functional substitution by homologous genes in order to compensate for the loss of RIG-I function.

For millions of years, viruses have coevolved with their hosts, leading to the development of various mechanisms for immune evasion in response to the mutual evolutionary pressure[13]. These

mechanisms involve the utilization of viral genes, proteins, and miRNA elements to counteract the host's innate immune response, cell apoptosis, and adaptive immunity[14]. Innate immunity functions as the initial defense against viral infection by identifying pathogenic components through PRRs. Consequently, the exploration of how viruses employ evolutionary strategies to evade different components of innate immunity, particularly through evasion of IFN responses, has garnered significant attention[15]. According to reports, viruses can employ various strategies to evade the immune system, including hiding their own genomic material, inhibiting critical host proteins, and modulating phosphorylation and ubiquitination pathways[16, 17]. For example, the encapsidation of the viral RNA by the viral nucleoprotein and polymerase prevents RIG-I binding and its subsequent activation[18]. Moreover, many viruses encode dsRNA-binding proteins (such as influenza virus NS1, vaccinia virus E3L, Ebola virus VP35, reovirus s3, bunya virus NSs, or herpes virus US11), which have been postulated to sequester the viral dsRNA from cellular dsRNA sensors[19]. In fish, there are also examples of viral immune escape, where they can utilize the immune evasion strategies mentioned above to escape IFN-mediated immune responses[20-22]. Recently, it is reported that N6-methyladenosine (m^6A) modification also plays a crucial role in enabling viruses to evade the interferon (IFN) response[23]. m^6A methylation is an important epigenetic modification that involves the dynamic and reversible process of RNA methylation, regulated by methylase (writer), demethylase (eraser), and reader proteins that recognize m^6A-modified RNA[24]. Viruses can not only use m^6A modification to hide themselves and avoid recognition by host receptors but also manipulate host gene expression through m^6A modification to enable immune evasion[25-27].

Fish and birds are commonly observed to exhibit "RIG-I deficiency" phenomena, and they are also the most abundant groups of aquatic and terrestrial vertebrates respectively, giving them certain evolutionary advantages. As a result, they are considered as a model group for studying the arms race between MDA5 receptors and 5'ppp-RNA, and researching the immune evolution of them helps us to understand the immune evolution of the entire vertebrates. Meanwhile, fish and birds are major source of high-quality protein for human consumption, viral diseases in aquaculture and livestock industry pose serious obstacles to the industry's healthy development. Among them, the 5’ppp-RNA virus, as mentioned earlier, is a highly pathogenic group. Within this group, siniperca cheats rhabdovirus (SCRV) is an important pathogen that can cause huge economic losses and serious threats to aquaculture in freshwater and marine fish. Therefore, in this study, we selected teleost fish miiuy croaker (*Miichthys miiuy*) and bird chicken (*Gallus gallus*), two vertebrates lacking RIG-I, to investigate the evolutionary strategies and interactions between 5’ppp-RNA virus and host. The final results demonstrated that fish MDA5 can recognize SCRV(one 5’ppp-RNA virus) and initiate signal transduction to activate IFN immune response, and the MDA5 of fish and birds lacking RIG-I both evolved the ability to recognize 5’ppp-RNA. In addition, SCRV can in turn utilize the m^6A strategy to degrade MDA5 for immune evasion. In summary, these findings shed light on the functional diversity of innate antiviral activity and unveil a complex arms race between virus replication and the innate immunity of its reservoir hosts in vertebrates. In addition, since the loss of RIG-I in vertebrates is a widespread event, our research also provides a new perspective for vertebrate groups that have lost RIG-I.

2. Results

2.1 A genetic compensation response model for RIG loss

In previous studies, it has been reported that a few vertebrates lost the RIG-I gene during evolution[8-10, 28]. To investigate this further, we utilized the recent advancements in available and comprehensive genomic data of vertebrates from the NCBI and Ensemble websites. By analyzing the genomes of various species, we determined the presence and absence of the RIG-I gene. As depicted in Figure 1A, the absence of the RIG-I gene does not appear to be uncommon in vertebrates, with at least three independent loss events observed in mammals, birds and fish, respectively. These gene-loss events occurred over a long evolutionary timescale. Based on the minimum age of the common ancestor of RIG-I-missing species (http://www.timetree.org/), the oldest recorded losses occurring in species like *Erpetoichthys calabaricus*, can be traced back to approximately 330 million years ago (MYA). Conversely, the detected loss in *Gallus gallus* took place less than 42 MYA. To gain a deeper understanding of the evolutionary dynamics of vertebrate RIG-I, we explored the conservation of the genes surrounding RIG-I. We analyzed the genome sequences of *Homo sapiens*, *Callorhinchus milii*, *Danio rerio*, *Tupaia belangeri*, *Gallus gallus*, and *M. miiuy* (Figure 1B). Similar to the slow-evolving *Callorhinchus milii*, humans possess RIG-I with TOPORS and ACO1 as its upstream and downstream genes, respectively. As previously reported[8, 9]. *Tupaia belangeri*, *Gallus gallus*, and *M. miiuy* do not have RIG-I. Interestingly, zebrafish has a RIG-I with its upstream gene being TOPORSb, seemingly a result of chromosome fragment duplication. However, the downstream gene of TOPORSa is missing a RIG-I, indicating that one of the RIG-I copies has been lost in zebrafish, similar to *M. miiuy*.

RIG-I plays a critical role in the innate immune system's response to viral infection, specifically by detecting 5’ppp-RNA viruses which are highly detrimental to vertebrate animals, thus the depletion of this gene is anticipated to greatly affect the immune response. Therefore, understanding the biological effects of RIG-I deficiency in vertebrates is essential for comprehending the origin and development of innate immunity. Homology-dependent genetic compensation response (HDGCR) is one of the important mechanisms through which GCR is achieved, and organisms often evolve the intelligent ability to compensate for the loss of a gene by utilizing homologous genes to compensate for the functional loss. In this study, we observed that teleost fish *M. miiuy*, one lower vertebrate, lacks the RIG-I gene. We conducted a protein structure analysis on *M. miiuy* MDA5 and LGP2, which are homologues of RIG-I, and observed that LGP2 lacks the CARD domain (Figure 1C), potentially rendering it unable to transmit signals but instead functioning as an intermediate regulator[7]. RIG-I’s specific recognition of 5’ppp-RNA prompted us to investigate whether MDA5, a structurally similar homolog to RIG-I, can substitute for RIG-I in recognizing 5'ppp-RNA in vertebrates without RIG-I (Figure 1D).

2.2 MDA5 promotes host antiviral innate immunity

To further investigate the alternative immune function of MDA5, we first investigated the fish MDA5-mediated signaling pathway in response to 5'ppp-RNA SCRV and double-stranded mimetic poly(I:C) infection. Two siRNA molecules (si-MDA5-1 and si-MDA5-2) were designed to assess the function of MDA5. si-MDA5-1 demonstrated higher inhibitory efficiency compared to si-MDA5-2 (Figure 2A). Therefore, si-MDA5-1 (referred to as si-MDA5) was selected for subsequent experiments. Subsequently, we constructed the MDA5 expression plasmid and

confirmed its cytoplasmic localization (Figure 2B). MDA5 is capable of binding not only to MAVS but also to STING to effectively transmit signals after virus infection (Figure 2C and 2D). Considering that mammalian MDA5 activates NF-κB and IRF3/IRF7 to induce IFNs, we investigated whether fish MDA5 could impact these pathways. Dual-luciferase reporter assays demonstrated that knockdown of MDA5 significantly inhibits NF-κB, IRF3, IRF7, and IFN-1 reporter genes (Figure 1E). In addition, we investigated the role of MDA5 in regulating the expression of IFN-stimulated genes (ISGs), which are crucial effectors. As shown in Figure 1F-1H, we observed that knockdown or overexpression of MDA5 can significantly inhibit or promote the expression levels of IFN-1, Mx1, ISG15, and Viperin upon SCRV or poly(I:C) infection. To visually represent the biological significance of MDA5 in SCRV-induced host cells, we utilized the virus plaque and qPCR methods to examine whether it could influence viral replication. As demonstrated in Figure 1I-1L, knockdown of MDA5 led to a significant increase in viral plaque formation and promoted SCRV replication in SCRV-infected cells, while overexpression had the opposite effect. Overall, these findings indicate that MDA5 plays a positive role in regulating the antiviral responses of teleost.

2.3 RD domain is required for MDA5 to recognize SCRV

We investigated whether *M. miiuy* MDA5, in the absence of RIG-I, can directly bind to the RNA of SCRV, a 5'ppp-RNA virus. To address this question, we precipitated the MDA5 protein from SCRV-infected MKC cells that were transfected with MDA5-Flag and pcDNA3.1-Flag. The bound RNA was then amplified using SCRV-specific primers or β-actin primers as a control. Our results showed that MDA5 interacted with SCRV, while β-actin mRNA did not associate with

MDA5 (Figure 3A). The C-terminal regulatory domain (RD) of RIG-I binds to viral RNA in a triphosphate-dependent manner, to determine if the RD domain of MDA5 has similar functions, we generated truncated mutations called MDA5-ΔRD and Western blot analysis confirmed the expression of MDA5 and MDA5-ΔRD plasmids (Figure 3B). We subsequently noted that MDA5-ΔRD exhibited an inability to interact with SCRV, which was supported by the loss of its immunological capability in inhibiting SCRV viral replication. (Figure 3C-3E). We also examined the effects of MDA5 and its mutant on antiviral factors in both uninfected and SCRV-infected MKC cells. In the absence of infection, overexpression of both MDA5 and MDA5-ΔRD stimulated the expression of antiviral genes (Figure 3F). However, when cells were infected with SCRV, only the overexpression of MDA5, not MDA5-ΔRD, significantly increased the expression of antiviral genes (Figure 3G). In summary, these findings provided evidence that MDA5 may recognize 5'-triphosphate-dependent RNA (5’ppp-RNA) through its RD domain.

2.4 MDA5 recognizes 5’ppp-RNA in vertebrates lacking RIG-I

To provide specific evidence of MDA5 recognition of 5’ppp-RNA in vertebrates lacking RIG-I, we synthesized 5’ppp-RNA and purified recombinant MDA5 of *Miichthys miiuy* and *Gallus gallus* (two species of vertebrates lacking RIG-I). 62 nt 5’ppp-RNA from the negative-strand RNA virus Vesicular Stomatitis Virus (VSV) and 112 bp dsRNA from the MDA5 gene sequence was generated through in vitro transcription using T7 polymerase. Gel analysis and nuclease sensitivity confirmed the generation of a single RNA product of the expected size (Figure 4A). The RNA pull-down experiment showed that 5’ppp-RNA can be recognized by *Miichthys miiuy* MDA5 (mmiMDA5), similar to 112 bp blunt end dsRNA which is one known MDA5 ligand

(Figure 4B). Furthermore, biotin-labeled 5’ppp-RNA captured mmiMDA5, while the biotin-labeled mutant types (5’-OH-RNA and 5’pppGG-RNA) did not (Figure 4C). Additionally, when recombinant mmiMDA5 was subjected to an electrophoresis mobility shift assay (EMSA) using a biotin-labeled 5’ppp-RNA probe, a clear complex was detected (Figure 4D and 4E). This complex formation was inhibited by adding an excess of cold 5’ppp-RNA but not 5’-OH-RNA and 5’pppGG-RNA, demonstrating the direct interaction between mmiMDA5 and 5’ppp-RNA (Figure 4E). Next, we investigated whether *Gallus gallus* MDA5 (ggaMDA5) shares the ability to recognize 5’ppp-RNA seen in fish, the RNA pull-down and EMSA experiments provided evidence that ggaMDA5 can also recognize 5’ppp-RNA (Figure 4F-4H). Overall, our findings demonstrated that MDA5 detection of RNA in RIG-I deficient vertebrates is guided by the RNA 5'-triphosphate end and is disrupted when RNA is capped at the 5'-triphosphate end or dephosphorylated.

2.5 Increased m^6A modification and expression of MDA5 upon SCRV infection

As stated in the previous results, MDA5 has evolved to possess immune recognition abilities that take over the role of RIG-I, significantly enhancing the host's ability to resist viral infections. However, evolution is a continuous battle between hosts and viruses, to counteract receptor recognition and immune responses by the host, viruses often evolve complex escape mechanisms to evade immune surveillance and destruction. Recently, studies have shown that the m^6A modification mechanism is a way that viruses can utilize to evade the immune response. To investigate the impact of SCRV infection on the overall methylation dynamics of fish hosts, we utilized methylated RNA immunoprecipitation sequencing (MeRIP-seq, GenBank accession number: PRJNA819945) to measure changes in m^6A modification of host transcripts during SCRV

infection (Figure 5A). From the results shown in Figure 5B, we identified 3060 differentially m^6A methylated peaks (p-value < 0.05) and 2082 differentially expressed genes (p-value < 0.05) between the non-infected and SCRV-infected group, indicating that infection significantly alters the m^6A modification of specific host transcripts. It is worth noting that hyper-methylated m^6A peaks were also observed in the MDA5 mRNA transcripts during SCRV infection (fold change >1.5, $p < 0.05$), and the expression level of MDA5 was higher in the infection group compared to the control group ($p < 0.05$). Further analysis of the m^6A-seq data showed that MDA5 contained m^6A sites in the exon1 region which were markedly higher in the infection group than that in the control group (Untreated VS SCRV: $p = 0.01$) (Figure 5C). Next, we tested the concrete m^6A modification sites of MDA5 mRNA. We used the SRAMP database to predict potential m^6A sites in MDA5-exon1 [30]. Four potential sites were predicted and two specific primers were designed (Figure 5D), then m^6A quantitative real-time PCR and semiquantitative PCR were performed. In line with the m^6A-seq data, the results further confirmed that m^6A sites exactly exist in MDA5 exon1 (Figure 5E). After being infected with SCRV or poly(I:C), the methylation level of MDA5 increased in MKC cells, further confirming the sequencing data (Figure 5F). Next, MDA5 was found to be upregulated in spleen and kidney tissues infected with SCRV (Figure 5G). We further explored the mRNA and protein levels of MDA5 in MKC cells infected with SCRV and poly(I:C) and found that their expression all first significantly increased and then returned to the normal level (Figure 5H and 5I). Overall, our results suggested that both the m^6A modification and expression levels of MDA5 are increased upon SCRV infection.

2.6 m^6A-modification weakens MDA5 mRNA stability and antiviral ability

SCRV infection can increase the methylation level of MDA5, and this mechanism is expected to have a regulatory effect on MDA5. To investigate this, the regulatory effects of METTL3 and METTL14, the main components of the methyltransferase complex, on MDA5 were explored. Three siRNAs targeting METTL3 and METTL14 were designed, and si-METTL3-2 and si-METTL14-3 showed higher knockdown efficiency (Figure 6A). METTL3 and METTL14-overexpressing plasmids were also constructed, and the interaction between them confirmed their cooperative role in m^6A modification (Figure 6B). Subsequently, the global m^6A levels were measured in cells after knockdown or overexpression of METTL3 and METTL14. Consistent with expectations, the knockdown of METTL3 and METTL14 significantly decreased the global m^6A level, while their overexpression significantly increased the overall methylation level (Figure 6C). To investigate their role in the process of virus infection, we used the virus plaque and qPCR methods to explore whether it could affect SCRV replication. As shown in Figure 6D and 6E, overexpression of METTL3 or METTL14 significantly enhances viral plaque formation and promotes SCRV replication in SCRV-infected cells. And as m^6A writers, METTL3 and METTL14 can directly regulate the methylation level of MDA5 and induce MDA5 degradation by reducing its mRNA stability (Figure 6F-6I). We further inserted the MDA5-exon1 into pmirGLO and mVenus-C1 vector, and results showed that si-METTL3&14 can reduce the luciferase activity of pmirGLO-MDA5-exon1, and METTL3&14 could suppress the levels of GFP, further indicating the presence of methylation sites in MDA5-exon1 (Figure 6-figure supplement 1A and 1D). To investigate the potential sites on MDA5-exon1, we constructed mutant MDA5-exon1 reporter plasmids. For the mutant form of MDA5-exon1 reporter genes, four predicted adenosine bases in m^6A consensus sequences (DRACH) were replaced by uracil, thus

canceling m^6A decoration (Figure 5D and Figure 6-figure supplement 1B). As expected, our results showed that the luciferase activity of wild-type pmirGLO-MDA5-exon1 reporter, but not of mutant pmirGLO-MDA5-exon1 reporter, was markedly increased upon METTL3&14 knockdown (Figure 6-figure supplement 1C). Furthermore, we found that the use of cycloleucine (CL, an amino acid analogue that can inhibit m^6A modification) hindered the degradation of MDA5 by METTL3 and METTL14, indicating that these proteins regulate MDA5 expression through a methylation mechanism (Figure 6J and 6K). Additionally, MDA5 expression was degraded by METTL3&14 in both SCRV-infected and uninfected groups (Figure 6L). To investigate the impact of this mechanism on viral infection, we co-transfected METTL3&14 and MDA5 plasmids and found that METTL3&14 partially suppressed the antiviral immune benefit of MDA5 (Figure 6M-6O). Taken together, our data demonstrate that METTL3&14-mediated m^6A methylation of MDA5 inhibits its mRNA stability and expression levels, thus suppressing the antiviral capabilities of MDA5.

2.7 Detailed m^6A regulatory mechanism of MDA5

The m^6A mechanism is jointly regulated by writers, erasers, and readers. The m^6A modification of mRNA recruits m^6A-binding proteins (readers) which have the function of recognizing m^6A sites and accelerating mRNA decay. In this study, we hypothesized that YTHDF readers (YTHDF1, YTHDF2, and YTHDF3) may recognize m^6A-modified MDA5 and destabilize it. We examined the binding ability of YTHDF proteins to MDA5 mRNA and found that YTHDF2 and YTHDF3 exhibited stronger binding compared to YTHDF1 (Figure 7A). We then designed two siRNAs targeting YTHDF1, YTHDF2, and YTHDF3 respectively, and selected si-YTHDF1-1,

si-YTHDF2-si-2, si-YTHDF3-2 with better knockdown effects for subsequent experiments (Figure 7B). Results showed that the knockdown or overexpression of YTHDF2 and YTHDF3 led to the increase or decrease of the expression levels of MDA5, whereas YTHDF1 did not appear to influence MDA5 expression (Figure 7C, 7D, Figure 7-figure supplement 1A and 1C). In addition, overexpression of YTHDF2&3 can increase the luciferase activity of wild-type pmirGLO-MDA5-exon1 reporter, but not of mutant pmirGLO-MDA5-exon1 reporter (Figure 7-figure supplement 1B). We then found that si-METTL3&14 can counteract the negative impact of YTHDF2&3 on MDA5 mRNA, protein, and stability (Figure 7E and 7F). Since the m^6A mechanism is reversible, we then studied the regulation of MDA5 by two major erasers. Results showed that FTO, not ALKBH5, can upregulate MDA5 expression (Figure 7G). Moreover, the overexpression of FTO can reverse the inhibitory effect of YTHDF2&3 on MDA5 (Figure 7H and 7I). Taken together, these data suggested that through METTL3&14-m^6A-YTHDF2&3 regulatory network, m^6A can mediate the degradation of MDA5, and this process can be countered by FTO (Figure 7J).

3. Discussion

In this study, we have identified multiple independent loss events of RIG-I throughout vertebrate evolution. Specifically, we have observed at least three independent loss events in mammals, birds, and fish, respectively. Regarding the loss of RIG-I in avian species, previous studies have provided more comprehensive and accurate information than ours, indicating that birds have experienced more than 16 instances of RIG-I loss[9]. However, it should be noted that we have not found the loss of RIG-I in reptiles and amphibians (not displayed). But this does not imply that there has been no loss event among them, but rather, there is insufficient information regarding the genomes of reptiles and amphibians to draw the conclusions. As the abundance of genomic data continues to grow, there will be an increasing amount of evidence available to verify the presence or absence of RIG-I in these taxonomic groups. Additionally, the presence of RIG-I in current species does not guarantee that RIG-I loss has not occurred previously. For instance, our research has indicated that zebrafish may have experienced RIG-I loss. However, prior to the loss event, the zebrafish RIG-I has undergone repetitive events. These findings collectively highlight that the loss of RIG-I is not a random occurrence, but rather bears significant biological and evolutionary implications that deserve further investigation.

The loss of RIG-I might be expected to have a great impact on immune response, and the evolutionary loss of it raises the question of a possible compensation of its function by other gene products. In this study, we characterized the consequences resulting from the loss of RIG-I in the vertebrate and provided direct functional evidence for the alternative immune recognition function of MDA5. Firstly, our results suggest that MDA5 of fish can bind to and recognize SCRV virus, leading to the activation of the RLR pathway and subsequent upregulation of antiviral factors,

thereby enhancing the host's antiviral immune capacity. SCRV belongs to the class of rhabdovirus, which is a negative-strand virus with a non-segmented genome and initiate both replication and transcription de novo leading to 5′-triphosphate RNA in the cytosol, was expected to trigger an IFN response without the need for replication and presumed dsRNA formation[4]. Consequently, we reasonably speculate that the recognition of SCRV by MDA5 depends on the 5’triphosphate of virus RNA in vertebrates that lacking RIG-I. Secondly, to further illustrate the above viewpoints, we synthesized 5’ppp-RNA and its dephosphorylated and capped forms and purified recombinant MDA5 of *Miichthys miiuy* and *Gallus gallus* (two representative species of vertebrates lacking RIG-I). Results demonstrated that MDA5 detection of RNA in RIG-I deficient vertebrates is guided by the RNA 5'-triphosphate and is disrupted when RNA is capped at the 5'-triphosphate end or dephosphorylated. Thirdly, the recognition of RNA by MDA5 depends on its RD domain, which not only indicates that the RD domain of MDA5 has evolved functions similar to RD domain of RIG-I, but also excludes the possibility of MDA5 binding to SCRV RNA through intermediate ligands. Furthermore, in vertebrates that possess RIG-I, STING exclusively binds to RIG-I rather than MDA5. In contrast, just like tree shrews and chickens lacking RIG [8, 30], the MDA5 of *M. miiuy* can also interact with STING protein, proving that in vertebrates lacking RIG-I, MDA5 can utilize STING to facilitate signal transduction in the antiviral response. Finally, by linking the immune replacement ability evolved by MDA5 with the common RIG-I loss event in vertebrates, we propose a straightforward explanation for this evolutionary event: In the lengthy process of vertebrate evolution, MDA5 gradually acquired new functionalities to effectively detect viruses such as 5’ppp-RNAs, which were initially recognized by RIG-I. As a result, there was functional redundancy of RIG-I, which eventually led to its gradual disappearance from the

vertebrate genome. This hypothesis is supported by two viewpoints: first, MDA5 and RIG-I can both recognize overlapping viruses[31]; secondly, in fish without RIG-I deficiency, MDA5 has stronger antiviral ability compared to RIG-I[32].

Viruses are constantly co-evolving with hosts. Our available data suggested that the vertebrate has evolved MDA5 with alternative functions to recognize and resist 5'ppp-RNA in the absence of RIG-I. As a response, virus has also evolved to use the m^6A mechanism to evade the host immune response. Previous study indicated that m^6A modification plays a crucial role in maintaining immune homeostasis in the body[33]. During the infection process, the virus may disrupt the m^6A level and disrupt the immune balance, thereby facilitating its own replication and invasion. Viruses may utilize the m^6A mechanism in two ways to evade immunity. On the one hand, many studies suggested a role for m^6A in shielding RNA species from detection by PRRs. There are numerous viruses recognized in RIG-I dependent manner, but m^6A modification increases the possibility of immune evasion. For example, the loss of m^6A site or removing m^6A from human metapneumovirus may weaken its immune evasion ability, prevent it from evading detection by RIG-I, and result in higher levels of IFN release[26]. Moreover, it has been reported that the RNA containing m^6A modifications binds to RIG-I poorly, and it failed to trigger the RIG-I conformational changes associated with downstream immune signals[34]. On the other hand, m^6A-mediated viral strategies for inhibiting IFN induction pathways appear to exist. For instance, following infection by human cytomegalovirus (HCMV), the IFN-β transcript was modified by m^6A, and this methylation decreased its half-life, suggesting that HCMV can exploit this control of IFN-β expression to facilitate its replication by increasing m^6A modification of the IFN-β transcript and thus decreasing its production[35]. Similarly, a previous study has reported that m^6A

modification levels significantly increase after T-cell infection with HIV-1, and this modification can enhance the replication and nucleation ability of the virus itself[36]. In summary, viruses can utilize m^6A to evade the immune response by shielding the recognition of RIG-I or reducing the host's immune reaction, thus counteracting the host's defense mechanisms. In our previous study, we discovered that SCRV infection can not only increase overall cellular methylation levels but also upregulate the expression of METTL3, thereby suggesting its potential to regulate host gene expression through the m^6A mechanism[38]. In this study, we found that SCRV virus infection alters m^6A modification of specific cellular transcripts, including MDA5. MDA5 plays a crucial role as a receptor in recognizing the SCRV virus and controlling IFN activation. The aberrant m^6A levels of MDA5 subsequently affect the expression of antiviral genes, thereby compromising its ability to mount an effective antiviral immune response. It is plausible that SCRV also impacts the production of antiviral genes, such as IFN-1 or other cytokines, by manipulating m^6A modification on the transcripts of cytokines or molecules involved in their production. This interesting aspect warrants further investigation in future research.

In this study, we demonstrated a co-evolutionary arms race between 5’ppp-RNA and virus receptors in vertebrates. Specifically, we conducted an evolutionary analysis and provided functional evidence to confirm that MDA5 of teleost fish and birds has acquired an additional function of sensing 5’ppp-RNA and enhancing the antiviral signaling pathway, thus compensating for the loss of RIG-I. Additionally, we found that SCRV infection can regulate the m^6A level of MDA5 in the host, leading to its degradation and subsequently affecting the immune response for immune evasion. Fish and birds, as the most abundant aquatic and terrestrial vertebrates respectively, are also the two lineages with the most frequent occurrence of RIG-I deficiency, the

investigation of host-pathogen interactions of them offers valuable insights into the ecological and evolutionary factors that contribute to the diversity of the immune system.

4. Materials and methods

4.1 Ethics statement

All animal experimental procedures were performed in accordance with the National Institutes of Health's Guide for the Care and Use of Laboratory Animals, and the experimental protocols were approved by the Research Ethics Committee of Shanghai Ocean University (No. SHOU-DW-2018-047).

4.2 Sample and challenge

M. miiuy (~50 g) was obtained from Zhoushan Fisheries Research Institute, Zhejiang Province, China. Fish was acclimated in aerated seawater tanks at 25℃ for six weeks before experiments. The experimental procedure for SCRV infection was performed as described[39].

4.3 Cell culture and treatment

M. miiuy kindey cells (MKCs), *M. miiuy* spleen cells (MPCs) were cultured in L-15 medium (HyClone) supplemented with 15% fetal bovine serum (FBS; Gibco), 100 U/ml penicillin, and 100μg/ml streptomycin at 26 °C. Fish EPC cells (Epithelioma papulosum cyprini cells) were maintained in medium 199 (Invitrogen) supplemented with 10% FBS, 100 U/ml penicillin, and 100 mg/ml streptomycin at 26 °C in 5% CO_2. HEK293 cells were cultured in DMEM (HyClone) supplemented with 10% FBS, 100 U/ml penicillin, and 100 mg/ml streptomycin at 37˚C in 5% CO_2. Chicken embryo fibroblast cells (DF-1) were cultured in DMEM (HyClone) supplemented with 10% FBS, 100 U/ml penicillin, and 100 mg/ml streptomycin at 39˚C in 5% CO_2. For stimulation experiments, Cells were challenged with SCRV at a multiplicity of infection (MOI) of

5 and harvested at different times for RNA extraction.

4.4 Oligonucleotides

The sequence of the 62 nt 5'ppp-RNA was derived from the 5' and 3'UTRs of the VSV genome as previously described[37], and the sequence of 112 bp dsRNA was taken from the first 100 bp of the MDA5 gene of miiuy croaker flanked by 5'-gggaga and tctccc-3'. 62 nt 5'ppp-RNA and 112 bp dsRNA were synthesized by in vitro transcription using the Ribo RNAmax-T7 kit (RiboBio). Biotin-labeled RNAs were transcribed in vitro using a Ribo RNAmax-T7 Biotin Labeling Transcription Kit (RiboBio). For generating duplexes, RNA oligonucleotides were mixed in hybridization buffer (20 mM Tris-HCl [pH 8.0], 1.5 mM MgCl2, and 1.5 mM DTT), boiled for 1 min, and incubated at 37 □ for 1 h. For removal of 5'-triphosphates, 20 mg of RNA was treated with 20 U Calf Intestinal Alkaline Phosphatase (CIAP, Invitrogen) for 2 h at 37 □ in the presence of RNase inhibitor (Beyotime) and extracted with phenolchloroform. RNA molecules with a terminal 5' m7G cap were synthesized by the incorporation of m7G cap analogue (Yeason) in the transcription reactions. RNA was analysed on a denaturing 17% polyacrylamide, 7 M urea gel following digestion with 50 ng/ul of RNase A (Beyotime) or 100 mU/ul of DNase I (Beyotime) for 30 min.

4.5 Plasmids construction

To construct Flag or Myc-tagged MAVS, STING, MDA5, METTL3, METTL14, FTO, ALKBH5, YTHDF1, YTHDF2, and YTHDF3 expression plasmids, their CDS sequences of the *M. miiuy* were amplified by PCR and then ligated into a pcDNA3.1 vector (Invitrogen), respectively.

Then, MDA5-△RD were generated by PCR on the basis of MDA5 plasmid. To construct MDA5-exon1 reporter vector, the exon1 region of *M. miiuy* MDA5 gene was amplified using PCR with the gene-specific primers and ligated into a pmir-GLO luciferase reporter vector (Promega). Meanwhile, *M. miiuy* MDA5-exon1 were inserted into the mVenus-C1 (Invitrogen), which included the sequence of enhanced GFP. For mutant reporter vectors (MDA5-exon1-mut), adenosine (A) in the predicted m^6A motif was replaced by an uracil (U) by using the Mut Express II Fast Mutagenesis Kit V2 (Vazyme) with specific primers 1). To construct Flag-tagged MDA5 expression plasmid of *G. gallus*, the CDS sequence of MDA5 was amplified by PCR and then ligated into a pcDNA3.1 vector (Invitrogen). For protein purification, MDA5 plasmids with 6× His tag was constructed based on pcDNA3.1. The correct construction of the recombinant plasmids was verified through Sanger sequencing and extracted using an Endotoxin-Free Plasmid DNA Miniprep Kit (Tiangen, China) before using plasmids. The primers were listed in Table S1.

4.6 Protein Purification and Analysis

(His6)-Flag-tagged MDA5 of *M. miiuy* and *G. gallus* were transiently overexpressed in 293T cells and lysed in a binding buffer (500 mM NaCl, 20 mM Tris/HCl [pH 7.4], 20 mM Imidazole, and 1% Triton X-100) including protease inhibitor cocktail (Roche). The lysate was incubated over night at 4 □ with anti-His beads (Solarbio). Anti-His beads were washed subsequently with washing buffer (500 mM NaCl, 20 mM Tris/HCl [pH 7.4], 20 mM Imidazole, and 1% Triton X-100). MDA5 proteins were eluted by an addtion of elution buffer (500 mM NaCl, 20 mM Tris/HCl [pH 7.4], 500 mM Imidazole, and 1% Triton X-100) to the beads. Purity of recombinant MDA5 was determined by SDS-PAGE separation and subsequent Coomassie bluestaining.

4.7 RNA interference

The MDA5-specific small interfering RNA (si-MDA5-1 and si-MDA5-2) sequences were 5'-CGGACUACAUGCAGCGUAATT-3' and 5'-GACCAAUGAGAUUUCUAUGTT-3', respectively. The METTL3-specific small interfering RNA (si-METTL3-1, si-METTL3-2, and si-METTL3-3) sequences were 5'-CAUCACAAACGAACUCAACTT-3', 5'-AACGUGGGCAAACUCUUUUTT-3' and 5'-GAGAUUCUGGAACUACUUATT-3', respectively. The METTL14-specific small interfering RNA (si-METTL14-1, si-METTL14-2, and si-METTL14-3) sequences were 5'-GCUGGAAAUCGAGGAGAUATT-3', 5'-CCGTACGAAGAGGTGTACATT-3' and 5'-GAGCCUCCCUUGGAAGAAUTT-3', respectively. The YTHDF1-specific small interfering RNA (si-YTHDF1-1 and si-YTHDF1-2) sequences were 5'-AAAGACUUUGACUGGAACUTT-3' and 5'-CAGUCGAUCAGAGACCUAATT-3', respectively. The YTHDF2-specific small interfering RNA (si-YTHDF2-1 and si-YTHDF2-2) sequences were 5'-GCAGGGUGUUUAUCAUCAATT-3', 5'-CUAUGCUCCCAGCUCAAUUTT-3', respectively. The YTHDF3-specific small interfering RNA (si-YTHDF3-1 and si-YTHDF3-2) sequences were 5'-GGUGGACUACAAUGCCUAUTT-3' and 5'-UCUACAGUAACAGCUAUGGTT-3', respectively. The scrambled control RNA sequences were 5' - UUCUCCGAACGUGUCACGUTT - 3'. They were purchased from GenePharma (Shanghai, China).

4.8 Cells transfection

Transient transfection of cells with siRNA was performed in 24-well plates using

Lipofectamine RNAiMAX (Invitrogen), and cells were transfected with DNA plasmids was performed using Lipofectamine 3000 (Invitrogen) according to the manufacturer's instructions. For functional analyses, the overexpression plasmid (500 ng per well) or control vector (500 ng per well) and siRNA (100 nM) were transfected into cells in culture medium and then harvested for further detection.

4.9 RNA extraction and quantitative real-time PCR

Total RNA was extracted using the TRIzol Reagent (Invitrogen) and the cDNA was synthesized using the FastQuant RT Kit (Tiangen) which contains DNase treatment of RNA to eliminate genomic contamination, following the manufacturer's instructions. The expression profiles of each gene were conducted by using the SYBR Premix Ex Taq™ (Takara), as previously described. The quantitative real-time PCR was conducted in an Applied Biosystems® QuantStudio 3 (Thermo Fisher Scientific). β-actin was used as internal controls for mRNA respectively. Primer sequences are listed in Table S1.

4.10 Western blotting

Cellular lysates were generated by using 1×SDS-PAGE loading buffer. Proteins were extracted from cells and measured with the BCA Protein Assay kit (Vazyme), then subjected to SDS-PAGE (10%) gel and transferred to PVDF (Millipore) membranes by semidry blotting (Bio-Rad Trans Blot Turbo System). The membranes were blocked with 5% BSA. Protein was blotted with different antibodies. The antibody against MDA5 was diluted at 1: 500 (Beyotime, Cat# AF7164); anti-Flag, anti-Myc and anti-Tubulin monoclonal antibody were diluted at 1: 1,000

(Sigma); and HRP-conjugated anti-rabbit IgG or anti-mouse IgG (Abbkine) at 1: 5,000. The results were the representative of three independent experiments. The immunoreactive proteins were detected by using WesternBright^{TM} ECL (Advansta). The digital imaging was performed with a cold CCD camera.

4.11 Dual-luciferase reporter assays

To determine the functional regulation of MDA5, MKC cells were co-transfected MDA5 expression plasmid, together with NF-κB, IRF3, IRF7, or IFN-1 luciferase reporter genes, and the pRL-TK *Renilla* luciferase reporter plasmid. After 48 h transfection, the cells were collected and lysed for reporter activity using the dual-luciferase reporter assay system (Promega). For the detection of m^6A site, the wild or mutant of MDA5-exon1 luciferase reporter was co-transfected si-METTL3, si-METTL14, si-YTHDF1, si-YTHDF2, si-YTHDF3 or si-Ctrl into MKC cells. After 48 h transfection, the cells were collected and lysed for the reporter luciferase activities measured by using a dual-luciferase reporter assay system (Promega). All the luciferase activity values were gained against the *Renilla* luciferase control. For each experiment, three independent experiments were conducted, and each experiment was done in triplicate.

4.12 RNA binding protein immunoprecipitation (RIP)

To identify whether MDA5 or MDA5-△RD can directly bind to SCRV viral RNA, MKC cells (~2.0×10^7) were transfected with pcDNA3.1-Flag, pcDNA3.1-MDA5-Flag or pcDNA3.1-MDA5-△RD-Flag and then infected with SCRV at an MOI of 5 for 24 h. In addition, to identify whether YTHDF1, YTHDF2, and YTHDF3 can directly bind to MDA5, MKC cells were co-transfected

with pcDNA3.1-Flag, pcDNA3.1-YTHDF1/2/3-Flag. For RNA immunoprecipitation (RIP) assays, MKC cells were harvested after 48 h transfection, and RIP assays were carried out with Magna RIP RNA-Binding Protein Immunoprecipitation Kit (Millipore) and anti-Flag antibody (Abcam) following the manufacturer's protocol. Then, the expression of target gene SCRV-M, SCRV-G, β-actin, or MDA5 were detected by quantitative real-time qRT-PCR analysis.

4.13 RNA Pull-Down assay

cytoplasmic extracts were prepared from 2 × 10^7 MKC cells transfected with mmiMDA5-Flag (MDA5 of miiuy croaker) plasmids and 5× 10^7 DF1 cells transfected with gga-MDA5-Flag (MDA5 of chicken) plasmids. The extracts were incubated with biotinylated 5'ppp-RNA or dsRNA and subjected to pull-down with streptavidin agarose beads (Geneseed), followed by subsequent Coomassie bluestaining or SDS-PAGE analysis and immunoblotting with anti-Flag antibody (Sigma) or MDA5 antibody (Boster).

4.14 EMSA assay

Recombinant MDA5 proteins were mixed with biotin-labeled oligonucleotides in a reaction mixture (10 μl: 20 mM Tris-HCl pH 8.0, 1.5 mM MgCl2, 1.5 mM DTT). After incubation at room temperature for 15 min, the reaction mixtures were conducted on 6 % non-denaturing polyacrylamide gels and the EMSA was performed using Chemiluminescent EMSA Kit (Beyotime).

4.15 MeRIP-seq assays and analysis

Total RNA was isolated using TRIzol reagent. m^6A immunoprecipitation and library preparation were performed following the manufacturer's protocol. Poly (A) RNA is purified from 50μg total RNA using Dynabeads Oligo (dT) (Thermo Fisher) using two rounds of purification. Then the poly(A) RNA was fragmented into small pieces using Magnesium RNA Fragmentation Module (NEB) under 86□ for 7 min. Then the cleaved RNA fragments were incubated for 2h at 4□ with m^6A-specific antibody (Synaptic Systems) in IP buffer (50 mM Tris-HCl, 750 mM NaCl and 0.5% Igepal CA-630). Then the IP RNA was reverse-transcribed to create the cDNA by SuperScript™ II Reverse Transcriptase (Invitrogen). The average insert size for the final cDNA library was 300±50 bp. For sequencing data analysis, we used HISAT2 to map reads to the reference genome of *M. miiuy*. Mapped reads of IP and input libraries were provided for R package exomePeak, which identifies m^6A peaks with bed or bigwig format that can be adapted for visualization on the IGV software. MEME and HOMER were used for de novo and known motif finding followed by localization of the motif with respect to peak summit. Called peaks were annotated by intersection with gene architecture using R package ChIPseeker. The differentially expressed mRNAs were selected with log2 (fold change) >1 or log2 (fold change) <-1 and *p*-value < 0.05 by R package edgeR. The circus map of m^6A peaks in untreated and SCRV-infected spleen tissues of *M. miiuy* was showed by TBtools[40].

4.16 MeRIP-qPCR

Total RNA was extracted using TRIzol reagent (Invitrogen). Methylated m^6A RNA immunoprecipitation (Me-RIP) was performed according to the protocol of EpiQuik™ CUT&RUN m^6A RNA Enrichment Kit (Epigentek). qPCR analysis of the methylated RNA was

performed to detect methylated MDA5 mRNA levels.

4.17 Total m^6A Quantification Assay

Total RNA was extracted by the TRIzol Reagent (Invitrogen). Then, an EpiQuik m^6A RNA Methylation Quantification Kit (EpiGentek) was used to detect the total m^6A level according to the manufacturer's protocol. Briefly, positive control (PC), negative control (NC), and 200 ng isolated mRNA were added to each well with the capture antibody. Next, the detection antibody was added. After several incubations, the m^6A level was quantified colorimetrically at a wavelength of 450 nm.

4.18 RNA stability assays

Cells were treated with actinomycin D (5 μg/mL) and then collected at different time points. RNA was extracted by TRIzol reagent (Invitrogen), and the mRNA levels were measured using qRT-PCR.

4.19 Database mining and sequence analysis

The species tree is constructed by submitting species names to the NCBI (https://www.ncbi.nlm.nih.gov/Taxonomy/CommonTree/wwwcmt.cgi). In order to determine whether there is RIG-I in vertebrates, we use *H. sapiens* and *D. rerio* RIG-I protein sequences to TBLASTN the whole genome sequence of the species on the ensemble website (http://www.ensemble.org/). In addition, in order to prevent the possibility of incomplete species genome, we also used RIG-I protein sequences of *H. sapiens* and *D. rerio* to compare the

transcriptome and genome sequenced of the designated species on NCBI website (http://www.ncbi.nlm.nih.gov/Genbank/). For further gene synteny analysis, RIG-I of *H. sapiens*, *C. milii*, *D. rerio* were used as anchor sites. In order to identify the MDA5 and LGP2 from *M. miiuy*, we used the homologues of zebrafish reported previously as queries to seek for the transcriptome[41] and a chromosome-scale genome database[42] of *M. miiuy* by using local TBLASTN and BLASTN programs, then the protein structures of MDA5 and LGP2 of *M. miiuy* were predicted by SMART website (http://smart.embl-heidelberg.de/).

4.20 Statistical analysis

Data are expressed as the mean ± SE from at least three independent triplicated experiments. . A two-sided Student's t test was used to evaluate the data. The relative gene expression data was acquired using the $2^{-\Delta\Delta CT}$ method, and comparisons between groups were analyzed by one-way analysis of variance (ANOVA) followed by Duncan's multiple comparison tests. A value of $p < 0.05$ was considered significant.

Acknowledgements

This study was supported by the National Natural Science Foundation of China (31822057).

Author contributions

S.G. designed and performed experiments, analyzed the data, performed bioinformatics analysis, and wrote the manuscript. X.L. performed experiments and provided advice in experimental plans. W.Z. provided advice in experimental plans. T.X. directed all the experiments and participated in experimental design, data analyses, interpretation, and manuscript writing.

Declaration of interests

The authors declare no competing interests.

References:

1. Pichlmair, A. & Sousa, C. R. E. Innate recognition of viruses. *Immunity* **27**, 370-383 (2007).
2. Yoneyama, M., et al. Shared and unique functions of the DExD/H-box helicases RIG-I, MDA5, and LGP2 in antiviral innate immunity. *Journal of Immunology* **175**, 2851-2858 (2005).
3. Kato, H., et al. Differential roles of MDA5 and RIG-I helicases in the recognition of RNA viruses. *Nature* **441**, 101-105 (2006).
4. Hornung, V., et al. 5 '-triphosphate RNA is the ligand for RIG-I. *Science* **314**, 994-997 (2006).
5. Loo, Y.-M. & Gale, M., Jr. Immune Signaling by RIG-I-like Receptors. *Immunity* **34**, 680-692 (2011).
6. Satoh, T., et al. LGP2 is a positive regulator of RIG-I- and MDA5-mediated antiviral responses. *Proceedings of the National Academy of Sciences of the United States of America* **107**, 1512-1517 (2010).
7. Saito, T., et al. Regulation of innate antiviral defenses through a shared repressor domain in RIG-I and LGP2. *Proceedings of the National Academy of Sciences of the United States of America* **104**, 582-587 (2007).
8. Xu, L., et al. Loss of RIG-I leads to a functional replacement with MDA5 in the Chinese tree shrew. *Proceedings of the National Academy of Sciences of the United States of America* **113**, 10950-10955 (2016).
9. Krchlikova, V., et al. Dynamic Evolution of Avian RNA Virus Sensors: Repeated Loss of RIG-I and RIPLET. *Viruses-Basel* **15**, (2023).

10. Liang, B. & Su, J. Advances in aquatic animal RIG-I-like receptors. *Fish and shellfish Immunology reports* **2**, 100012-100012 (2021).

11. Walker, P. J., et al. ICTV Virus Taxonomy Profile: Rhabdoviridae 2022. *Journal of General Virology* **103**, (2022).

12. Millet, J. K., Jaimes, J. A. & Whittaker, G. R. Molecular diversity of coronavirus host cell entry receptors. *Fems Microbiology Reviews* **45**, 10.1093/femsre/fuaa057 (2021).

13. Naz, S. S., Aslam, A. & Malik, T. An Overview of Immune Evasion Strategies of DNA and RNA Viruses. *Infectious disorders drug targets* **21**, e300821192322 (2021).

14. Felix, J. & Savvides, S. N. Mechanisms of immunomodulation by mammalian and viral decoy receptors: insights from structures. *Nature Reviews Immunology* **17**, 112-129 (2017).

15. Garcia-Sastre, A. Ten Strategies of Interferon Evasion by Viruses. *Cell Host & Microbe* **22**, 176-184 (2017).

16. Schulz, K. S. & Mossman, K. L. Viral Evasion Strategies in Type I IFN Signaling - A Summary of Recent Developments. *Frontiers in Immunology* **7**, 498 (2016).

17. Ke, F. & Zhang, Q.-Y. Aquatic animal viruses mediated immune evasion in their host. *Fish & Shellfish Immunology* **86**, 1096-1105 (2019).

18. Weber, M., et al. Influenza Virus Adaptation PB2-627K Modulates Nucleocapsid Inhibition by the Pathogen Sensor RIG-I. *Cell Host & Microbe* **17**, 309-319 (2015).

19. Versteeg, G. A. & Garcia-Sastre, A. Viral tricks to grid-lock the type I interferon system. *Current Opinion in Microbiology* **13**, 508-516 (2010).

20. Li, S., et al. The P Protein of Spring Viremia of Carp Virus Negatively Regulates the Fish Interferon Response by Inhibiting the Kinase Activity of TANK-Binding Kinase 1. *Journal of*

Virology **90**, 10728-10737 (2016).

21. Ke, Q., et al. Role of Viral Hemorrhagic Septicemia Virus Matrix (M) Protein in Suppressing Host Transcription. *Journal of Virology* **91**, 10.1128/JVI.00279-17 (2017).

22. Thoulouze, M. I., Bouguyon, E., Carpentier, C. & Bremont, M. Essential role of the NV protein of Novirhabdovirus for pathogenicity in rainbow trout. *Journal of Virology* **78**, 4098-4107 (2004).

23. Lou, X., Wang, J.-J., Wei, Y.-Q. & Sun, J.-J. Emerging role of RNA modification N6-methyladenosine in immune evasion. *Cell Death & Disease* **12**, 300 (2021).

24. Shi, H., Wei, J. & He, C. Where, When, and How: Context-Dependent Functions of RNA Methylation Writers, Readers, and Erasers. *Molecular Cell* **74**, 640-650 (2019).

25. Zhang, Y., et al. RNA-binding protein YTHDF3 suppresses interferon-dependent antiviral responses by promoting FOXO3 translation. *Proceedings of the National Academy of Sciences of the United States of America* **116**, 976-981 (2019).

26. Lu, M., et al. N-6-methyladenosine modification enables viral RNA to escape recognition by RNA sensor RIG-I. *Nature Microbiology* **5**, 584-+ (2020).

27. Wu, J., et al. N6-Methyladenosine Modification Opens a New Chapter in Circular RNA Biology. *Frontiers in Cell and Developmental Biology* **9**, 709299 (2021).

28. Chen, S. N., Zou, P. F. & Nie, P. Retinoic acid-inducible gene I (RIG-I)-like receptors (RLRs) in fish: current knowledge and future perspectives. *Immunology* **151**, 16-25 (2017).

29. Zhou, Y., Zeng, P., Li, Y.-H., Zhang, Z. & Cui, Q. SRAMP: prediction of mammalian N-6-methyladenosine (m(6)A) sites based on sequence-derived features. *Nucleic Acids Research* **44**, (2016).

30. Xu, L., Yu, D., Fan, Y., Liu, Y.-P. & Yao, Y.-G. Evolutionary selection on MDA5 and LGP2 in the chicken preserves antiviral competence in the absence of RIG-I. *Journal of Genetics and Genomics* **46**, 499-503 (2019).

31. Schoggins, J. W., et al. A diverse range of gene products are effectors of the type I interferon antiviral response (vol 472, pg 481, 2011). *Nature* **525**, 10.1038/nature14554 (2015).

32. Wan, Q., Yang, C., Rao, Y., Liao, Z. & Su, J. MDA5 Induces a Stronger Interferon Response than RIG-I to GCRV Infection through a Mechanism Involving the Phosphorylation and Dimerization of IRF3 and IRF7 in CIK Cells. *Frontiers in Immunology* **8**, 189 (2017).

33. Gan, L., Zhao, Y., Fu, Y. & Chen, Q. The potential role of m6A modifications on immune cells and immunotherapy. *Biomedicine & Pharmacotherapy* **160**, 114343 (2023).

34. Durbin, A. F., Wang, C., Marcotrigiano, J. & Gehrke, L. RNAs Containing Modified Nucleotides Fail To Trigger RIG-I Conformational Changes for Innate Immune Signaling. *Mbio* **7**, e00833-16 (2016).

35. Rubio, R. M., Depledge, D. P., Bianco, C., Thompson, L. & Mohr, I. RNA m(6)A modification enzymes shape innate responses to DNA by regulating interferon beta. *Genes & Development* **32**, 1472-1484 (2018).

36. Tirumuru, N. & Wu, L. HIV-1 envelope proteins up-regulate N-6-methyladenosine levels of cellular RNA independently of viral replication. *Journal of Biological Chemistry* **294**, 3249-3260 (2019).

37. Goulet, M.-L., et al. Systems Analysis of a RIG-I Agonist Inducing Broad Spectrum Inhibition of Virus Infectivity. Plos Pathogens 9, (2013).

38. Geng, S., et al. The m6A Reader YTHDF2 Modulates Antiviral and Antibacterial Activity by

Suppressing METTL3 Methylation-Modified STING in Fish. *Journal of immunology (Baltimore, Md. : 1950)* **210**, 653-667 (2023).

39. Chu, Q., Xu, T., Zheng, W., Chang, R. & Zhang, L. Long noncoding RNA MARL regulates antiviral responses through suppression miR-122-dependent MAVS downregulation in lower vertebrates. *Plos Pathogens* **16**, e1008670 (2020).

40. Chen, C., et al. TBtools: An Integrative Toolkit Developed for Interactive Analyses of Big Biological Data. *Molecular Plant* **13**, 1194-1202 (2020).

41. Che, R. B., Sun, Y. Y., Sun, D. Q. & Xu, T. J. Characterization of the Miiuy Croaker (Miichthys miiuy) Transcriptome and Development of Immune-Relevant Genes and Molecular Markers. *Plos One* **9**, e94046 (2014).

42. Xu, T., Li, Y., Zheng, W., & Sun, Y. A chromosome-level genome assembly of the miiuy croaker (*Miichthys miiuy*) using nanopore sequencing and Hi-C. *Aquaculture and Fisheries*. 10.1016/j.aaf.2021.06.001 (2021).

Figure Legends:

Figure 1. A genetic compensation response model for RIG loss. (A) Loss of RIG-I in vertebrates. Each branch tip represents one species. Red lines show lineages where loss of RIG-I. The red circle indicates the occurrence of an independent loss event. Branch lengths scale in millions of years (MYA). (B) Comparative analysis of gene synteny of RIG-I in vertebrate genomes. (C) Predicted protein structures of MDA5 and LGP2 in *M. miiuy*. (D) A genetic compensation response model for RIG loss.

Figure 2. MDA5 promotes host antiviral innate immunity. (A) Silence efficiency of si-MDA5 measured by qRT-PCR and Western blotting. Two siRNAs of MDA5 were transfected into MPC cells for 48 h respectively. (B) subcellular localization of MDA5 in MKCs by immunofluorescence. (C and D) MDA5 immunoprecipitates with MAVS (C) and STING (D). EPC cells (1×10^7) were co-transfected with MAVS-Myc or STING-Myc and MDA5-Flag expression plasmids for 24 h, followed by immunoprecipitation (IP) with anti-Myc. (E) MDA5 knockdown suppresses NF-κB, IRF3, IRF7, and IFN-1 signaling. MPC cells were transfected with pRL-TK Renilla luciferase plasmid, luciferase reporter genes, together with MDA5 expression plasmid. At 48 h post-transaction, the luciferase activity was measured and normalized to renilla luciferase activity. (F) Knockdown of MDA5 attenuates the expression of antiviral genes. MPC cells were transfected with si-Ctrl or si-MDA5 for 24 h and then treated with SCRV or poly (I:C) for 24 h. The expression of IFN-1, Mx1, ISG15, and Viperin expression were determined by qPCR. (G and H) Overexpression of MDA5 promotes the expression of antiviral genes. MKC cells were transfected with vector or MDA5 expression plasmid for 24 h and then treated with SCRV or poly

(I:C) for 24 h. The expression of MDA5(G), and antiviral genes, including IFN-1, Mx1, ISG15, and Viperin (H) were determined by qPCR. (I and K) MPC cells transfected with si-Ctrl or si-MDA5 and MKC cells transfected with pcDNA3.1 vector or MDA5 plasmid 24 h and then treated with SCRV at the dose indicated for 48 h. Then, cell monolayers were fixed with 4% paraformaldehyde and stained with 1% crystal violet. (J and L) MDA5 inhibits SCRV replication. MPC cells were transfected with si-Ctrl or si-MDA5 and MKC cells were transfected with pcDNA3.1 vector or MDA5 expression plasmid for 24 h, then infected with SCRV for 12, 24, or 48 h. The qPCR analysis was conducted for SCRV-M and SCRV-G RNA levels. All data presented as the means ± SE from at least three independent triplicated experiments. **, $p < 0.01$; *, $p < 0.05$ versus the controls.

Figure 3. RD domain is required for MDA5 to recognize SCRV. (A) The association of MDA5 proteins with SCRV. (B) Schematics and expression of MDA5 and truncated MDA5 (MDA5-△RD). (C) The association of MDA5 and MDA5-△RD proteins with SCRV. (D) MKC cells transfected with pcDNA3.1 vector, MDA5, or MDA5-△RD plasmids for 24 h and then treated with SCRV at the dose indicated for 48 h. Then, cell monolayers were fixed with 4% paraformaldehyde and stained with 1% crystal violet. (E) MKC cells were transfected with pcDNA3.1 vector, MDA5 or MDA5-△RD expression plasmids for 24 h, then infected with SCRV for 24 h, then the qPCR analysis was conducted for SCRV-M and SCRV-G RNA levels. (F and G) Expression of MDA5 and antiviral genes in uninfected or SCRV-infected MKC cells transfected with pcDNA3.1 vector, MDA5, or MDA5-△RD expression plasmids. All data presented as the means ± SE from at least three independent triplicated experiments. **, $p < 0.01$; *, $p < 0.05$

versus the controls.

Figure 4. MDA5 recognize 5'ppp-RNA in vertebrates lacking RIG-I. (A) Schematic representation of 5'ppp-RNA and dsRNA. The product of in vitro transcription runs as a single product degraded by RNase I. (B) Pulldown of dsRNA and 5'ppp-RNA by mmiMDA5. MKC cells were transfected with mmiMDA5-Flag plasmid, and the input and immunoprecipitated MDA5 proteins were analyzed by Coomassie bluestaining and Western blot. (C) The cytoplasmic fraction of MKC cells transfected with Flag-tagged mmiMDA5 was incubated with biotinylated 5'ppp-RNA, 5'OH-RNA (5'ppp-RNA dephosphorylated by CIAP), or 5'pppGG-RNA (5'ppp-RNA capped by m7G cap analog). RNA-protein complexes were pulled down using streptavidin affinity beads. Input and pull-down samples were analyzed by SDS-PAGE and immunoblotting using anti-Flag and anti-MDA5 antibody. (D) Purity of recombinant mmiMDA5 was determined by Coomassie bluestaining. (E) EMSA of 5'ppp-RNA with mmiMDA5. For binding competition, indicated unlabeled RNAs (50-fold molar excess over the probe) were included. (F) Pulldown of dsRNA and 5'ppp-RNA by ggaMDA5. DF-1 cells were transfected with ggaMDA5-Flag plasmid, and the input and immunoprecipitated MDA5 proteins were analyzed by Western blot. (G) The cytoplasmic fraction of DF-1 cells transfected with Flag-tagged ggaMDA5 was incubated with biotinylated 5'ppp-RNA, 5'OH-RNA (5'ppp-RNA dephosphorylated by CIAP), or 5'pppGG-RNA (5'ppp-RNA capped by m7G cap analog). RNA-protein complexes were pulled down using streptavidin affinity beads. Input and pull-down samples were analyzed by SDS-PAGE and immunoblotting using anti-Flag antibody. (H) EMSA of 5'ppp-RNA with ggaMDA5. For binding competition, indicated unlabeled RNAs (50-fold molar excess over the

probe) were included.

Figure 5. Increased m^6A modification and expression of MDA5 upon SCRV infection. (A) Schematic of the MeRIP-seq protocol used to identify differential m^6A methylation following infection of *M. miiuy* spleen tissues with SCRV. (B) Circos plots showing differentially m^6A-methylated peaks identified from normal and SCRV-infected spleen tissues of *M. miiuy*. The green and red lines on the innermost ring represented the m^6A peaks identified from normal and SCRV-infected spleen tissues of *M. miiuy* respectively. The orange lines represent the log2 fold change values for each differentially m^6A peak. The blue spots represent the fold change of gene expression. Chromosomes were shown on the outermost ring, the ruler on which represented the physical distance is in millions of bases (Mb). (C) The m^6A abundance in MDA5 mRNA transcripts detected by MeRIP-seq, the m^6A peak of MDA5 is circled in the green box. (D) The exon1 sequence of MDA5 was submitted to the SRAMP website, and then the predicted m^6A site was displayed. Four predicted methylation sites located on the exon1 of MDA5 were marked by red box, then we designed two m^6A specific primers (MDA5-m^6A-1 and MDA5-m^6A-2). (E) m^6A abundance on MDA5 exon1 detected by MeRIP-qPCR and emiquantitative PCR in MKC cells. (F) MeRIP-qRT-PCR analysis of relative m^6A level of MDA5 in Mock, SCRV, and poly(I:C)-infected MKC cells. (G) mRNA levels of MDA5 in spleen and kidney tissues measured by qRT-PCR at indicated time after SCRV and infection. (H and I) mRNA and protein levels of MDA5 in MKC cells measured by qRT-PCR and Western blotting at indicated time after SCRV (H) and poly(I:C) (I) infection. All data presented as the means ± SE from at least three independent triplicated experiments. **, $p < 0.01$ versus the controls.

Figure 6. m^6A-modification weakens MDA5 mRNA stability and antiviral ability. (A) Silence efficiency of si-METTL3 and si-METTL14 measured. Three siRNAs of METTL3 and METTL14 were transfected into MPC cells for 48 h respectively. (B) METTL3 immunoprecipitates with METTL14. EPC cells (1×10^7) were co-transfected with METTL3-Myc and METTL14-Flag expression plasmids for 24 h, followed by immunoprecipitation (IP) with anti-Myc. (C) METTL3 and METTL14 significantly increased the m^6A content. MPCs were transfected with si-Ctrl or si-METTL3 or si-METTL14 and MKCs were transfected with vector or METTL3 or METTL14 plasmids for 48 h, then the m^6A level was measured by colorimetry. (D) METTL3 and METTL14 overexpressed MKC cells seeded in 48-well plates overnight were treated with SCRV at the dose indicated for 48 h. Then, cell monolayers were fixed with 4% paraformaldehyde and stained with 1% crystal violet. (E) MKC cells were transfected with pcDNA3.1 vector and METTL3 or METTL14 expression plasmid for 24 h, then infected with SCRV for 24 h. The qPCR analysis was conducted for SCRV-M and SCRV-G RNA levels. (F) The m^6A level alteration of MDA5 upon METTL3 or METTL14 knockdown or overexpression was examined by MeRIP-qPCR. MPC cells were transfected with si-Ctrl or si-METT3 and MKC cells were transfected with vector or METTL3 or METTL14 plasmids for 48 h. (G and H) MPC cells were transfected with si-Ctrl, si-METTL3 or METTL14 and MKC cells were transfected with vector, METTL3, or METTL14 plasmids for 48 h, the expression of MDA5 was detected by qRT-PCR and Western blotting. (I) MPC cells were transfected with si-Ctrl, si-METTL3, or si-METTL14, and MKC cells were transfected with vector, METTL3, or METTL14 plasmids, then 5 μg/ml actinomycin D was added to the cells for 0 h, 2 h, and 4 h. The half-life of MDA5 was analyzed by qRT-PCR. (J) MKC cells

were transfected with vector or METTL3&14 plasmids for 24 h and then treated with Cycloleucine (CL) for 24 h in a final concentration of 20 mM. The expression of MDA5 was detected by qRT-PCR and Western blotting. (K) MKC cells were transfected with vector or METTL3&14 plasmids for 24 h and then treated with CL for 24 h at 20 mM, then 5 μg/ml actinomycin D was added to the cells for 0 h, 2 h, and 4 h. The half-life of MDA5 was analyzed by qRT-PCR. (L) MKC cells were transfected with vector or METTL3&14 plasmids for 24 h and stimulated with SCRV for 24 h, then the expression of MDA5 was detected by qRT-PCR and Western blotting. (M) MKC cells seeded in 48-well plates overnight were transfected with MDA5 or MDA5+METTL3&14 plasmids for 48 h, then the expression of MDA5 was detected by qRT-PCR and Western blotting. (N) MKC cells seeded in 48-well plates overnight were transfected with MDA5 or MDA5+METTL3&14 plasmids were treated with SCRV at the dose indicated for 48 h. Then, cell monolayers were fixed with 4% paraformaldehyde and stained with 1% crystal violet. (O) MKC cells were transfected with MDA5 or MDA5 + METTL3&14 plasmids for 24 h, then infected with SCRV for 24 h. The qPCR analysis was conducted for SCRV-M and SCRV-G RNA levels. All data presented as the means ± SE from at least three independent triplicated experiments. **, $p < 0.01$; *, $p < 0.05$ versus the controls.

Figure 7. Detailed m^{6}A regulatory mechanism of MDA5. (A) The binding relationship between YTHDF1, YTHDF2, or YTHDF3 and MDA5 mRNA was validated using a RIP assay. MKC cells were transfected with YTHDF1-Flag, YTHDF2-Flag, YTHDF3-Flag, or pcDNA3.1-Flag for 48 h. (B) SiRNA silencing effect test of YTHDF1, YTHDF2, and YTHDF3. MPC cells were transfected with si-YTHDF1, si-YTHDF2, or si-YTHDF3 for 48 h. (C and D) MPC cells were transfected

with si-YTHDF1, si-YTHDF2, si-YTHDF3 or si-Ctrl (C), and MKC cells were transfected with YTHDF1, YTHDF2, YTHDF3 or vector for 48 h (D), then the expression of MDA5 was detected by qRT-PCR and Western blotting. (E) Relative mRNA and protein levels of MDA5 in MKC cells after co-transfected with YTHDF2&3 plasmids and si-METTL3&14 by qPCR and western blot assays. (F) MKC cells were transfected with YTHDF2&3 plasmids and si-METTL3&14, then 5 μg/ml actinomycin D was added to the cells for 0 h, 2 h, and 4 h. The half-life of MDA5 was analyzed by qRT-PCR. (G) MKC cells were transfected with vector, FTO, ALKBH5 plasmids for 48 h, then the expression of MDA5 was detected by qRT-PCR and Western blotting. (H) Relative mRNA and protein levels of MDA5 in MKC cells after co-transfected with YTHDF2&3 plasmids and FTO plasmids by qPCR and western blotting. (I) MKC cells were transfected with YTHDF2&3 plasmids and FTO plasmids, then 5 μg/ml actinomycin D was added to the cells for 0 h, 2 h, and 4 h. The half-life of MDA5 was analyzed by qRT-PCR. (J) Schematic diagram of arms race between MDA5 and 5'ppp-RNA.

Supporting Information

Supplementary file 1. PCR primer information in this study.

Figure 6-figure supplement 1. The regulation of m^6A writers (METTL3&14) to the MDA5-exon1. (A) Relative luciferase activity of pmirGLO-MDA5-exon1 firefly luciferase reporters in MPC cells transfected with si-Ctrl, si-METTL3 or si-METTL14. (B) Schematic diagram of m^6A site mutation on exon1 of MDA5. 'A' in the predicted methylation motif was replaced by 'U'. (C) Relative luciferase activity of wild-type or mutant pmirGLO-MDA5-exon1

firefly luciferase reporter in MPC cells transfected with si-Ctrl or si-METTL3&14. (D) METTL3 and METTL14 could downregulate GFP expression of mVenus-MDA5-exon1. EPC cells were co-transfected with the mVenus-MDA5-exon1 and vector, METTL3 or METTL14 plasmids. At 48 h post-transfection, the fluorescence intensity and the GFP expression were evaluated by enzyme-labeled instrument and western blotting, respectively. All data presented as the means ± SE from at least three independent triplicated experiments. **, $p < 0.01$ versus the controls.

Figure 7-figure supplement 1. The regulation of YTHDF readers (YTHDF1&2&3) to the MDA5-exon1. (A) Relative luciferase activity of pmirGLO-MDA5-exon1 firefly luciferase reporters in MPC cells transfected with si-Ctrl, si-YTHDF1, si-YTHDF2 or si-YTHDF3. (B) Relative luciferase activity of wild-type or mutant pmirGLO-MDA5-exon1 plasmids in MPC cells transfected with si-Ctrl or si-YTHDF2&3. (C) YTHDF2 and YTHDF3 could downregulate GFP expression of mVenus-MDA5-exon1. EPC cells were co-transfected with the mVenus-MDA5-exon1 and vector, YTHDF1, YTHDF2 or YTHDF3 plasmids. At 48 h post-transfection, the fluorescence intensity and the GFP expression were evaluated by enzyme-labeled instrument and western blotting, respectively. All data presented as the means ± SE from at least three independent triplicated experiments. **, $p < 0.01$ versus the controls.

Figure 1

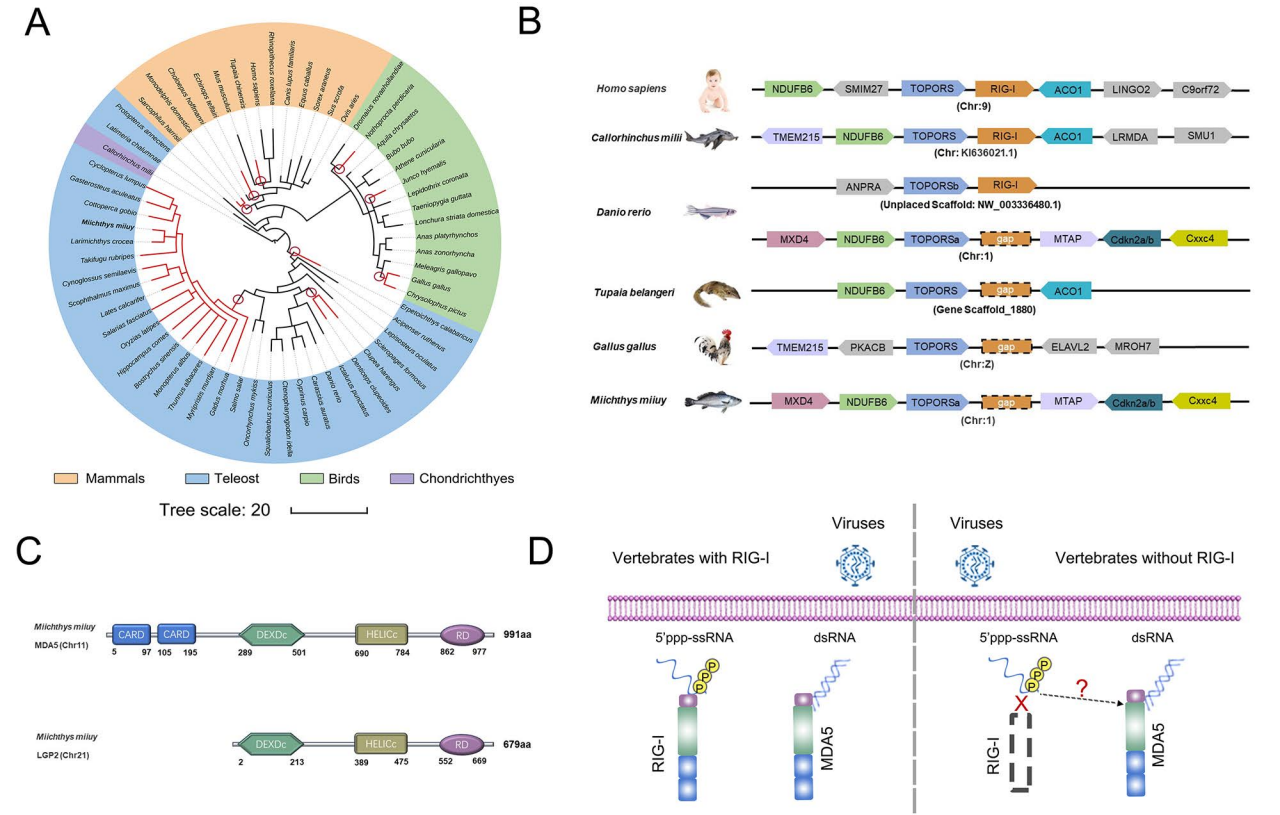
A
Mammals
Teleost
Birds
Chondrichthyes
Tree scale: 20
B
Homo sapiens
NDUFB6
SMIM27
TOPORS
RIG-I
ACO1
LINGO2
C9orf72
(Chr:9)
Callorhinchus milii
TMEM215
NDUFB6
TOPORS
RIG-I
ACO1
LRMDA
SMU1
(Chr: KI636021.1)
Danio rerio
ANPRA
TOPORSb
RIG-I
(Unplaced Scaffold: NW_003336480.1)
MXD4
NDUFB6
TOPORSa
gap
MTAP
Cdkn2a/b
Cxxc4
(Chr:1)
Tupaia belangeri
NDUFB6
TOPORS
gap
ACO1
(Gene Scaffold_1880)
Gallus gallus
TMEM215
PKACB
TOPORS
gap
ELAVL2
MROH7
(Chr:Z)
Miichthys miiuy
MXD4
NDUFB6
TOPORSa
gap
MTAP
Cdkn2a/b
Cxxc4
(Chr:1)
C
Miichthys miiuy
MDA5 (Chr11)
CARD
CARD
DEXDc
HELICc
RD
991aa
5
97
105
195
289
501
690
784
862
977
Miichthys miiuy
LGP2 (Chr21)
DEXDc
HELICc
RD
679aa
2
213
389
475
552
669
D
Viruses
Vertebrates with RIG-I
Viruses
Vertebrates without RIG-I
5'ppp-ssRNA
dsRNA
5'ppp-ssRNA
dsRNA
RIG-I
MDA5
RIG-I
MDA5

Figure 2

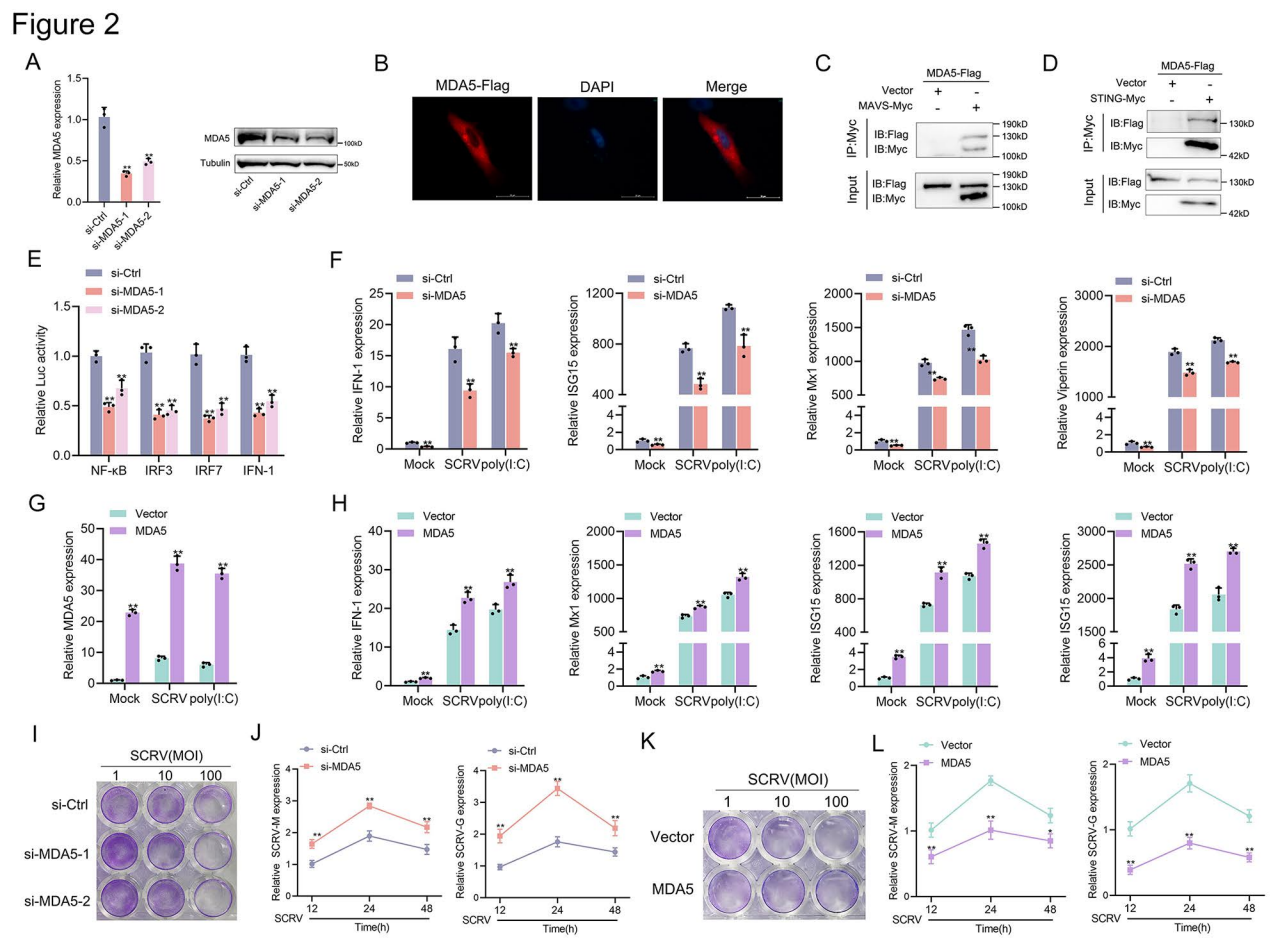
A
Relative MDA5 expression
si-Ctrl
si-MDA5-1
si-MDA5-2
MDA5
Tubulin
100kD
50kD
B
MDA5-Flag
DAPI
Merge
C
MDA5-Flag
Vector
MAVS-Myc
IP:Myc
IB:Flag
IB:Myc
Input
190kD
130kD
100kD
D
MDA5-Flag
Vector
STING-Myc
IP:Myc
IB:Flag
IB:Myc
Input
130kD
42kD
E
si-Ctrl
si-MDA5-1
si-MDA5-2
Relative Luc activity
NF-κB
IRF3
IRF7
IFN-1
F
si-Ctrl
si-MDA5
Relative IFN-1 expression
Relative ISG15 expression
Relative Mx1 expression
Relative Viperin expression
Mock
SCRV
poly(I:C)
G
Vector
MDA5
Relative MDA5 expression
H
Relative IFN-1 expression
Relative Mx1 expression
Relative ISG15 expression
Relative ISG15 expression
I
SCRV(MOI)
1
10
100
si-Ctrl
si-MDA5-1
si-MDA5-2
J
si-Ctrl
si-MDA5
Relative SCRV-M expression
Relative SCRV-G expression
SCRV
Time(h)
K
SCRV(MOI)
Vector
MDA5
L
Vector
MDA5
Relative SCRV-M expression
Relative SCRV-G expression
SCRV
Time(h)

Figure 3

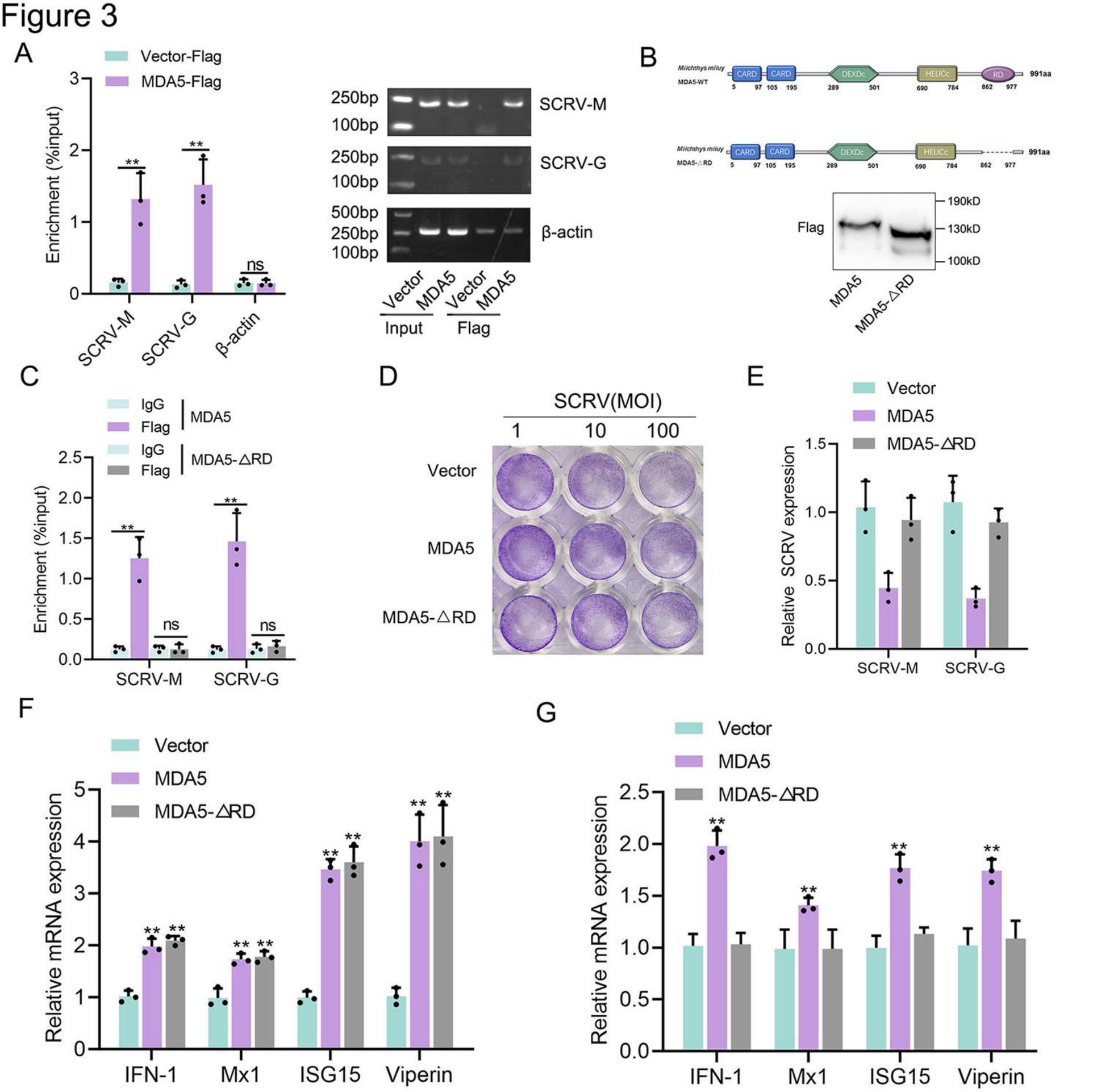
A
Vector-Flag
MDA5-Flag
Enrichment (%input)
SCRV-M
SCRV-G
β-actin
250bp
100bp
500bp
Vector
MDA5
Input
Flag
B
Miichthys miluy
MDA5-WT
CARD
DEXDc
HELICc
RD
991aa
MDA5-△RD
Flag
190kD
130kD
100kD
C
IgG
Flag
MDA5
MDA5-△RD
ns
D
SCRV(MOI)
1
10
100
Vector
MDA5
MDA5-△RD
E
Relative SCRV expression
F
Relative mRNA expression
IFN-1
Mx1
ISG15
Viperin
G

Figure 4

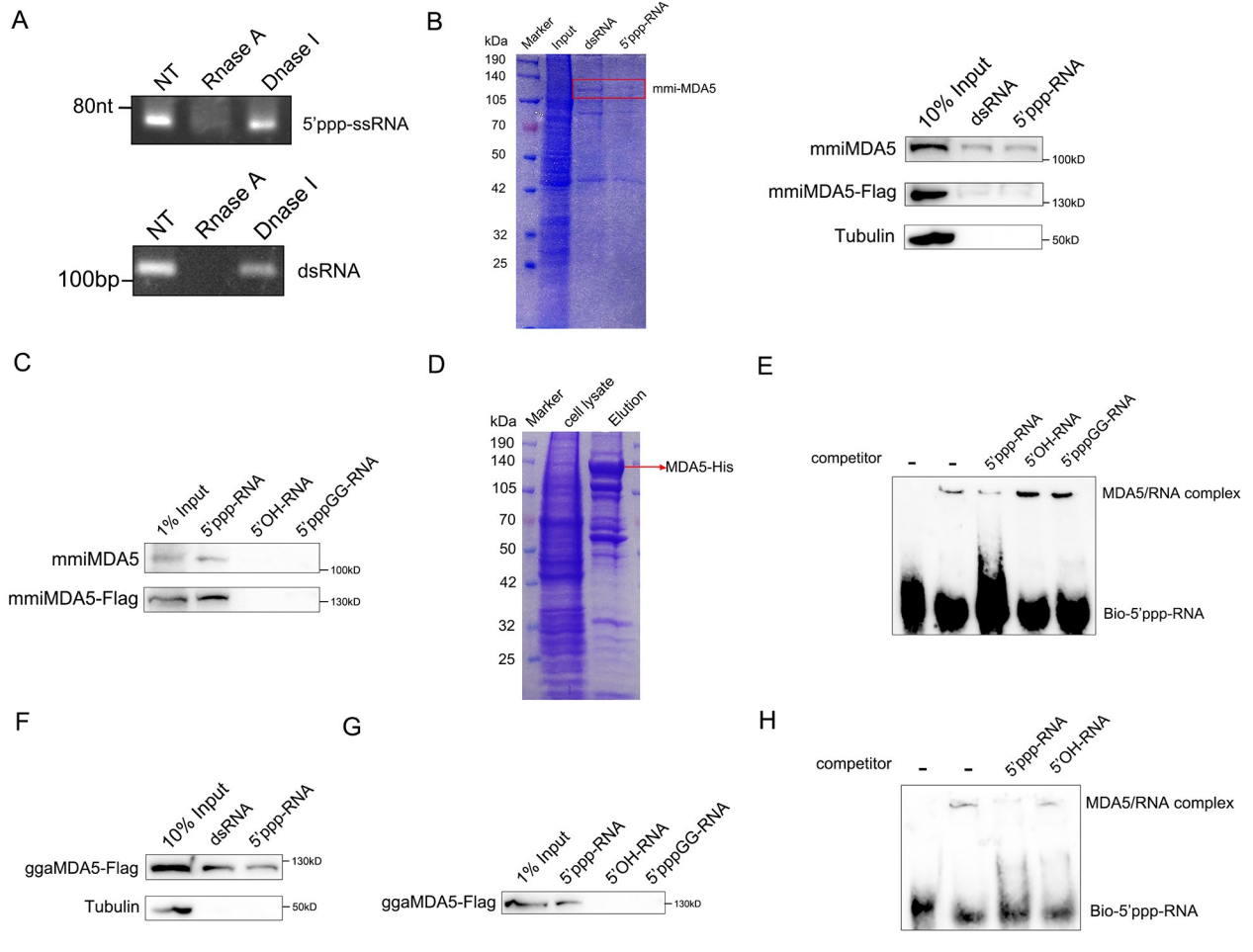
A
NT
Rnase A
Dnase I
80nt
5'ppp-ssRNA
NT
Rnase A
Dnase I
100bp
dsRNA
B
kDa
Marker
Input
dsRNA
5'ppp-RNA
190
140
105
70
50
42
32
25
mmi-MDA5
10% Input
dsRNA
5'ppp-RNA
mmiMDA5
100kD
mmiMDA5-Flag
130kD
Tubulin
50kD
C
1% Input
5'ppp-RNA
5'OH-RNA
5'pppGG-RNA
mmiMDA5
100kD
mmiMDA5-Flag
130kD
D
kDa
Marker
cell lysate
Elution
190
140
105
70
50
42
32
25
MDA5-His
E
competitor
-
-
5'ppp-RNA
5'OH-RNA
5'pppGG-RNA
MDA5/RNA complex
Bio-5'ppp-RNA
F
10% Input
dsRNA
5'ppp-RNA
ggaMDA5-Flag
130kD
Tubulin
50kD
G
1% Input
5'ppp-RNA
5'OH-RNA
5'pppGG-RNA
ggaMDA5-Flag
130kD
H
competitor
-
-
5'ppp-RNA
5'OH-RNA
MDA5/RNA complex
Bio-5'ppp-RNA

Figure 5

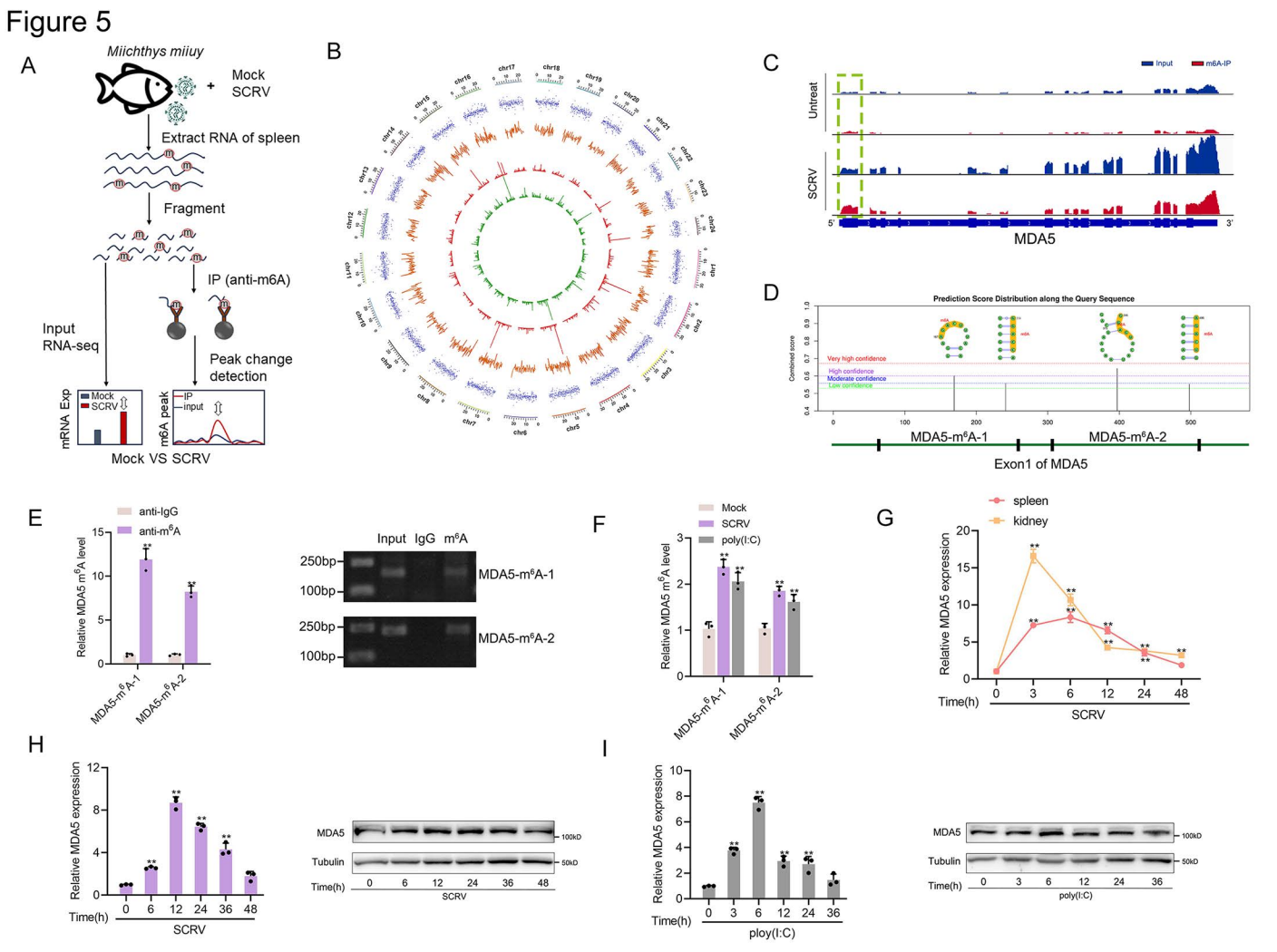
A
Miichthys miiuy
Mock
SCRV
Extract RNA of spleen
Fragment
IP (anti-m6A)
Input
RNA-seq
Peak change
detection
mRNA Exp
Mock
SCRV
m6A peak
IP
input
Mock VS SCRV
B
C
Input
m6A-IP
Untreat
SCRV
5'
3'
MDA5
D
Prediction Score Distribution along the Query Sequence
Combined score
Very high confidence
High confidence
Moderate confidence
Low confidence
MDA5-m6A-1
MDA5-m6A-2
Exon1 of MDA5
E
anti-IgG
anti-m6A
Relative MDA5 m6A level
MDA5-m6A-1
MDA5-m6A-2
Input
IgG
m6A
250bp
100bp
F
Mock
SCRV
poly(I:C)
Relative MDA5 m6A level
G
spleen
kidney
Relative MDA5 expression
Time(h)
SCRV
H
Relative MDA5 expression
Time(h)
SCRV
MDA5
Tubulin
100kD
50kD
I
Relative MDA5 expression
ploy(I:C)
poly(I:C)

Figure 6

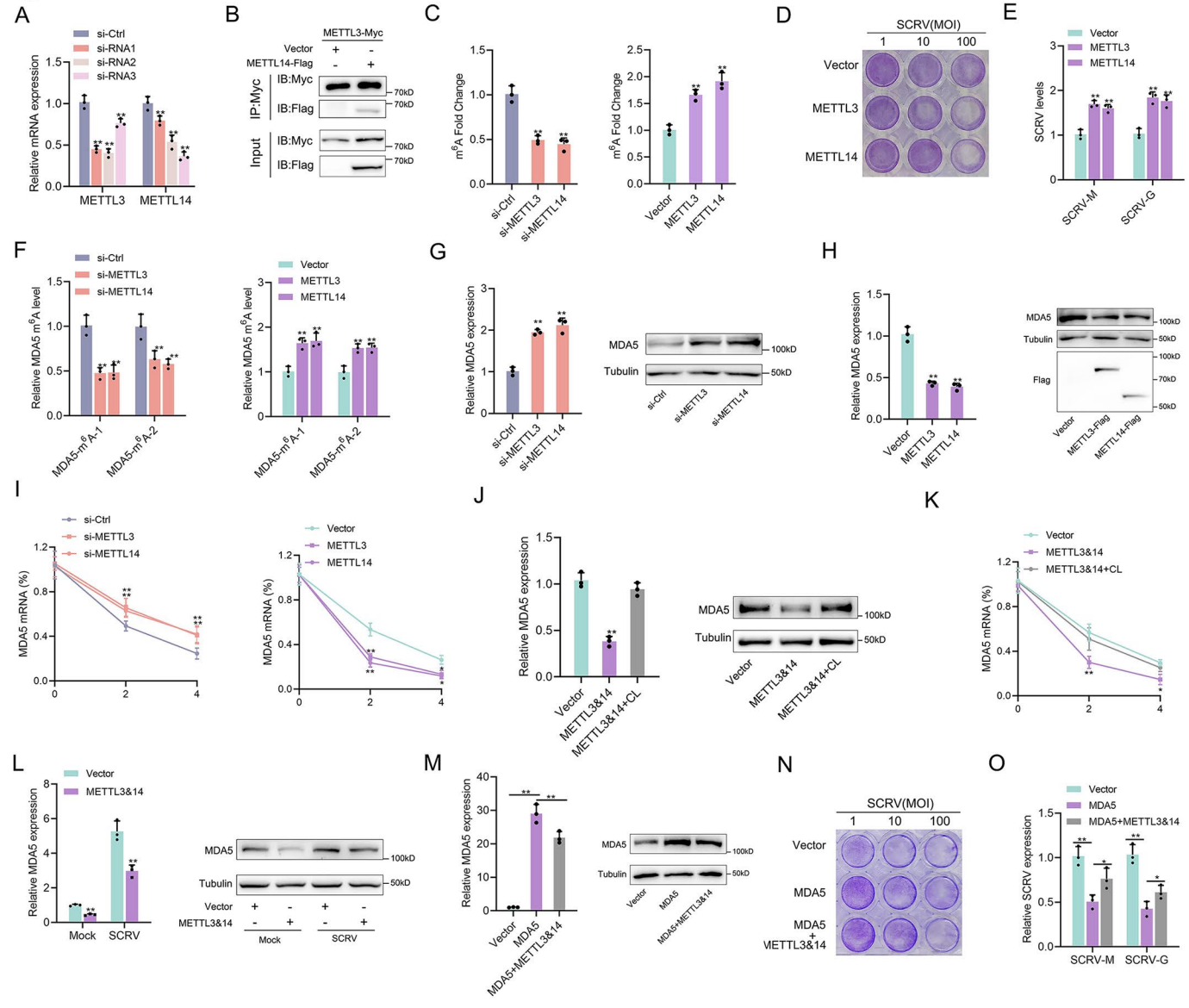
A
si-Ctrl
si-RNA1
si-RNA2
si-RNA3
Relative mRNA expression
METTL3
METTL14
B
METTL3-Myc
Vector
METTL14-Flag
IP:Myc
IB:Myc
IB:Flag
Input
70kD
C
m6A Fold Change
si-Ctrl
si-METTL3
si-METTL14
Vector
METTL3
METTL14
D
SCRV(MOI)
1
10
100
Vector
METTL3
METTL14
E
SCRV levels
SCRV-M
SCRV-G
F
si-Ctrl
si-METTL3
si-METTL14
Relative MDA5 m6A level
MDA5-m6A-1
MDA5-m6A-2
Vector
METTL3
METTL14
G
Relative MDA5 expression
MDA5
Tubulin
100kD
50kD
H
Relative MDA5 expression
Flag
METTL3-Flag
METTL14-Flag
I
MDA5 mRNA (%)
J
Relative MDA5 expression
Vector
METTL3&14
METTL3&14+CL
K
MDA5 mRNA (%)
L
Relative MDA5 expression
Mock
SCRV
M
Relative MDA5 expression
MDA5+METTL3&14
N
O
Relative SCRV expression

Figure 7

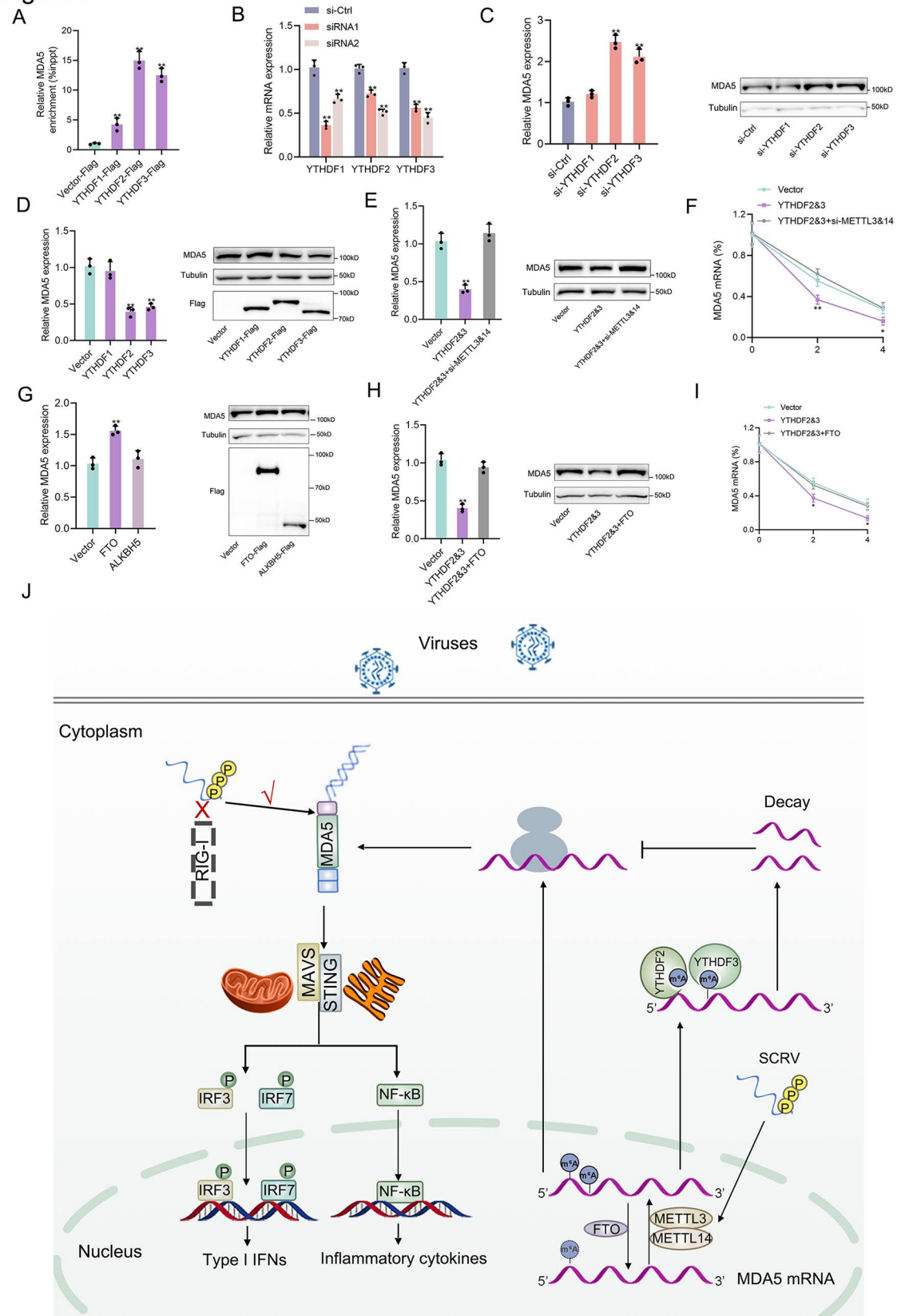
A
Relative MDA5 enrichment (%input)
Vector-Flag
YTHDF1-Flag
YTHDF2-Flag
YTHDF3-Flag
B
si-Ctrl
siRNA1
siRNA2
Relative mRNA expression
YTHDF1
YTHDF2
YTHDF3
C
Relative MDA5 expression
si-Ctrl
si-YTHDF1
si-YTHDF2
si-YTHDF3
MDA5
Tubulin
100kD
50kD
D
Relative MDA5 expression
Vector
YTHDF1
YTHDF2
YTHDF3
Flag
70kD
E
YTHDF2&3
YTHDF2&3+si-METTL3&14
F
YTHDF2&3+si-METTL3&14
MDA5 mRNA (%)
G
FTO
ALKBH5
FTO-Flag
ALKBH5-Flag
H
YTHDF2&3+FTO
I
J
Viruses
Cytoplasm
RIG-I
MDA5
MAVS
STING
IRF3
IRF7
NF-κB
Nucleus
Type I IFNs
Inflammatory cytokines
Decay
YTHDF2
YTHDF3
m6A
5'
3'
SCRV
FTO
METTL3
METTL14
MDA5 mRNA